EUROPEAN ORGANIZATION FOR NUCLEAR RESEARCH (CERN)

FERMILAB-PUB-15-376-CMS

CERN-PH-EP/2015-113
2015/09/01

CMS-HIG-14-016

Measurement of differential cross sections for Higgs boson production in the diphoton decay channel in pp collisions at $\sqrt{s} = 8\,\text{TeV}$

The CMS Collaboration*

arXiv:1508.07819v1 [hep-ex] 31 Aug 2015

Abstract

A measurement is presented of differential cross sections for the Higgs boson (H) production in pp collisions at $\sqrt{s} = 8\,\text{TeV}$. The analysis exploits the $\text{H} \to \gamma\gamma$ decay in data corresponding to an integrated luminosity of $19.7\,\text{fb}^{-1}$ collected by the CMS experiment at the LHC. The cross section is measured as a function of the kinematic properties of the diphoton system and of the associated jets. Results corrected for detector effects are compared with predictions at next-to-leading order and next-to-next-to-leading order in perturbative quantum chromodynamics, as well as with predictions beyond the standard model. For isolated photons with pseudorapidities $|\eta| < 2.5$, and with the photon of largest and next-to-largest transverse momentum (p_{T}^{γ}) divided by the diphoton mass $m_{\gamma\gamma}$ satisfying the respective conditions of $p_{\text{T}}^{\gamma}/m_{\gamma\gamma} > 1/3$ and $>1/4$, the total fiducial cross section is $32 \pm 10\,\text{fb}$.

Submitted to the European Physical Journal C

© 2015 CERN for the benefit of the CMS Collaboration. CC-BY-3.0 license

*See Appendix B for the list of collaboration members

1 Introduction

In 2012, the ATLAS and CMS Collaborations announced the observation [1–3] of a new boson with a mass of about 125 GeV, with properties consistent with expectations for the standard model (SM) Higgs boson. The Higgs boson (H) is the particle predicted to exist as a consequence of the spontaneous symmetry breaking mechanism acting in the electroweak sector of the SM [4–6]. This mechanism was suggested more than fifty years ago, and introduces a complex scalar field, which gives masses to W and Z bosons [7–11]. The scalar field also gives mass to the fundamental fermions through a Yukawa interaction [5]. Couplings and spin of the new boson are found to be consistent with the SM predictions [12–16]. A measurement of the $\mathrm{pp} \to \mathrm{H} \to \gamma\gamma$ differential cross section as a function of kinematic observables investigates possible deviations in distributions related to production, decay, and additional jet activity. It provides a check of perturbative calculations in quantum chromodynamics (QCD), and can point to alternative models in the Higgs sector. A similar analysis has been carried out by the ATLAS Collaboration in diphoton and four-lepton decay channels [17–19].

Despite its small branching fraction of ≈0.2% [20] predicted by the SM, the $\mathrm{H} \to \gamma\gamma$ decay channel provides a clean final-state topology and a precise reconstruction of the diphoton mass. The dominant background arises from irreducible direct-diphoton production and from the reducible $\mathrm{pp} \to \gamma$+jets and $\mathrm{pp} \to$ jets final states. The relatively high efficiency of the $\mathrm{H} \to \gamma\gamma$ selection makes this final state one of the most important channels for observing and investigating the properties of the new boson.

In this paper, the cross section is measured as a function of the kinematic properties of the diphoton system, and, in events with at least one or two accompanying jets, also as a function of jet-related observables. Two isolated photons are required to be within pseudorapidities $|\eta| < 2.5$, and the photon with largest and next-to-largest transverse momentum (p_{T}^{γ}) must satisfy the respective conditions of $p_{\mathrm{T}}^{\gamma}/m_{\gamma\gamma} > 1/3$ and $>1/4$, where $m_{\gamma\gamma}$ represents the diphoton mass. The transverse momentum $p_{\mathrm{T}}^{\gamma\gamma}$ and the rapidity $|y^{\gamma\gamma}|$ of the Higgs boson, observables related to the opening angle between the two photons, and the number of jets N_{jets} with $p_{\mathrm{T}} > 25\,\mathrm{GeV}$ produced in association with the diphoton system, are defined in this inclusive fiducial selection. A departure relative to the SM-predicted angular distributions would be an important observation, as it could reflect different spin and parity properties [21] than expected in the SM.

The variables defined with at least one accompanying jet are sensitive to the transverse Lorentz boost of the diphoton system. A modification in the corresponding distributions or in the $p_{\mathrm{T}}^{\gamma\gamma}$ spectrum could signify new contributions to gluon-gluon fusion production of the Higgs boson (ggH) [22]. The variables defined by requiring at least two accompanying jets are related to production of $\mathrm{H} \to \gamma\gamma$ through vector boson fusion (VBF); however, given the low event yield after selecting two jets, no other selection is applied to enhance this production mechanism. This is different from what was done in Ref. [12], where an attempt was made to classify the events according to the production mechanism. The differential cross sections are therefore mainly sensitive to the dominant ggH production mode of the Higgs boson.

The data correspond to an integrated luminosity of $19.7\,\mathrm{fb}^{-1}$ collected at the CERN LHC by the CMS experiment in proton-proton collisions at $\sqrt{s} = 8\,\mathrm{TeV}$. The trigger requirements and vertex determination are identical to those of Ref. [12], while photon selection and event classification are modified to reduce their dependence on p_{T}^{γ} and η^{γ}, providing thereby a less model-dependent measurement. Photons are identified using a multivariate classifier that combines information on distributions of shower and isolation variables designed to be independent of p_{T}^{γ} and η^{γ}. The signal yield is extracted by fitting the $m_{\gamma\gamma}$ distribution simultaneously in all bins

of the observables. To improve the sensitivity of the analysis, the selected events are categorized using an estimator of the mass resolution that is not correlated with $m_{\gamma\gamma}$, which simplifies the description of the background. Measured distributions are unfolded for detector effects and compared to distributions at the generator level from latest Monte Carlo (MC) predictions.

The paper is organized as follows. After a brief description of the CMS detector and event reconstruction given in Section 2, and of the simulated samples in Section 3, the photon selection and event classification are detailed in Section 4, where we also describe the kinematic observables. Section 5 provides the statistical methodology for extracting the signal, and gives details on modelling signal and background, and on the unfolding procedure. Systematic uncertainties are detailed in Section 6. Unfolded results are then compared with theoretical predictions in Section 7, and a brief summary is given in Section 8.

2 The CMS detector

A full description of the CMS detector, together with a definition of the coordinate system and the relevant kinematic variables, can be found in Ref. [23]. Its central feature is a superconducting solenoid, 13 m in length and 6 m in diameter, which provides an axial magnetic field of 3.8 T. The core of the solenoid is instrumented with trackers and calorimeters. The steel flux-return yoke outside the solenoid is equipped with gas-ionisation detectors used to reconstruct and identify muons. Charged-particle trajectories are measured using silicon pixel and strip trackers, within $|\eta| < 2.5$. A lead tungstate crystal electromagnetic calorimeter (ECAL) and a brass and scintillator hadron calorimeter (HCAL) surround the tracking volume and cover the region $|\eta| < 3$. The ECAL barrel extends to $|\eta| < 1.48$, while the ECAL endcaps cover the region $1.48 < |\eta| < 3.0$. A lead and silicon-strip preshower detector is located in front of each ECAL endcap in the region $1.65 < |\eta| < 2.6$. The preshower detector includes two planes of silicon sensors that measure the transverse coordinates of the impinging particles. A steel and quartz-fibre Cherenkov calorimeter extends the coverage to $|\eta| < 5.0$. In the (η, ϕ) plane, for $|\eta| < 1.48$, the HCAL cells map onto 5×5 ECAL crystal arrays to form calorimeter towers projecting radially outwards from points slightly offset from the nominal interaction point. In the endcap, the ECAL arrays matching the HCAL cells contain fewer crystals. To optimize the energy resolution, the calorimeter signals are calibrated and corrected for several detector effects [24]. Calibration of the ECAL uses the ϕ-symmetry of the energy flow, photons from $\pi^0 \to \gamma\gamma$ and $\eta \to \gamma\gamma$, and electrons from $\mathrm{W} \to \mathrm{e}\nu$ and $\mathrm{Z} \to \mathrm{e}^+\mathrm{e}^-$ decays. Changes in the transparency of the ECAL crystals due to irradiation during the LHC running periods and their subsequent recovery are monitored continuously and corrected, using light injected from a laser system.

Photons are reconstructed from clusters of energy deposition into so-called "superclusters" in the ECAL [25]. Events are selected using triggers requiring two photons with different thresholds in energy in the transverse plane (E_T), respectively, $E_\mathrm{T} > 26$ and >18 GeV for the leading and subleading photons, and through other complementary selections. One selection requires a loose calorimetric identification based on the distribution in energy in the electromagnetic cluster, and loose isolation requirements on photon candidates. The other selection requires a photon candidate to have a high value of R_9 variable, defined as the sum of the energies deposited in the array of 3×3 crystals centred on the crystal with highest energy deposition in the supercluster, divided by the energy of the supercluster. Photons that convert to $\mathrm{e}^+\mathrm{e}^-$ pairs before reaching the calorimeter tend to have wider showers and smaller values of R_9 than unconverted photons. High trigger efficiency is maintained by having both photons satisfy either selection. The measured trigger efficiency is 99.4% for events satisfying the diphoton

preselections described in Section 4.

3 Monte Carlo samples

The MC simulation of detector response employs a detailed description of the CMS detector, and uses GEANT4 version 9.4.p03 [26]. Simulated events include additional pp collisions that take place in or close to the time span of the bunch crossing, and overlap the interaction of interest. The probability distribution of these pileup events is weighted to reproduce the observed number of interactions in data.

The MC samples for ggH and VBF processes use the next-to-leading order (NLO) matrix element generator POWHEG (version 1.0) [27–31] interfaced with PYTHIA 6.426 [32]. The CT10 [33] set of parton distribution functions (PDF) is used in the calculation. The POWHEG generator is tuned following the recommendations of Ref. [34] and reproduces the Higgs boson p_{T} spectrum predicted by the HqT calculation [35, 36]. The PYTHIA 6 tune Z2* is used to simulate the hadronization and underlying event in pp collisions at 8 TeV. The Z2* tune is derived from the Z1 tune [37], which uses the CTEQ5L PDF, whereas Z2* adopts CTEQ6L1 [38]. The cross section for the ggH process is reduced by 2.5% for all values of m_{H} to accommodate its interference with nonresonant diphoton production [39]. The PYTHIA 6 generator is used alone for the VH (where V represents either the W or Z boson) and $\mathrm{t\bar{t}H}$ processes with the CTEQ6L1 PDF [38] and Z2* tune. The SM cross sections and branching fractions are taken from Ref. [20].

The samples of Drell–Yan events ($\mathrm{q\bar{q}} \to \mathrm{Z}/\gamma^* \to \ell^+\ell^-$, where ℓ is a lepton), and background samples used to represent the diphoton continuum and processes where one of the photon candidates arises from misidentified jet fragments, are the same as used in Ref. [12]. Simulated samples of $\mathrm{Z} \to \mathrm{e}^+\mathrm{e}^-$, $\mathrm{Z} \to \mu^+\mu^-$, and $\mathrm{Z} \to \mu^+\mu^-\gamma$ events, used for comparison with data and to extract an energy scale and corrections for resolution of photon energies, are generated with MADGRAPH, SHERPA, and POWHEG [40], providing comparisons among the different generators. Simulated background samples are used for training of multivariate discriminants, and for defining selection and classification criteria.

The diphoton continuum processes involving two prompt photons are simulated using SHERPA 1.4.2 [41]. The remaining processes where one of the photon candidates arises from misidentified jet fragments are simulated using PYTHIA 6 alone.

A comparison of unfolded data with results from models for ggH using the MC generators HRES [42, 43], POWHEG and POWHEG+MINLO [44], and MADGRAPH5_aMC@NLO [45] is presented in Section 7.

4 Event selection and classification

Trigger requirements, vertex determination, and kinematic criteria on photons are unchanged relative to those given in Ref. [12]. The multivariate classifiers used to identify photons and to estimate mass resolution are also unchanged, but used in a different way. Instead of using a discriminant for photon identification as an input to the final diphoton kinematic discriminant, a requirement is set on the photon identification discriminant. Event classification, instead of being based on the output of the kinematic discriminant, is based on the estimated $m_{\gamma\gamma}$ resolution. These differences are described in greater detail in the following section.

4.1 Photon identification

Photon candidates are required to be within the fiducial region of $|\eta| < 2.5$, excluding the barrel–endcap transition region of $1.44 < |\eta| < 1.57$, where photon reconstruction is not optimal. The transverse momenta of the two photons are required to satisfy the previously mentioned conditions of $p_{\mathrm{T}}^{\gamma 1}/m_{\gamma\gamma} > 1/3$ and $p_{\mathrm{T}}^{\gamma 2}/m_{\gamma\gamma} > 1/4$. The use of p_{T} thresholds scaled by $m_{\gamma\gamma}$ prevents the distortion of the low end of the $m_{\gamma\gamma}$ spectrum that results if a fixed threshold is used. Photons are also required to satisfy preselection criteria based on isolation and distributions in shower variables slightly more stringent than used in the trigger requirements.

Three variables are calculated for each reconstructed candidate for a pp interaction vertex: the sum of the p_{T}^2 of the charged-particle tracks emerging from the vertex, and two variables that quantify the difference in the vector and scalar sums in p_{T} between the diphoton system and the charged-particle tracks associated with the vertex. In addition, if either photon is associated with any charged-particle track identified as resulting from $\gamma \to \mathrm{e}^+\mathrm{e}^-$ conversion, extrapolation of their trajectories is used to clarify the origin of the vertex of their production. These variables are used as inputs to a multivariate system based on a boosted decision tree (BDT) classifier to choose the reconstructed vertex to associate with the diphoton system. All BDTs are implemented using the TMVA [46] framework.

Another BDT is trained to separate prompt photons from photon candidates resulting from misidentification of jet fragments passing the preselection requirements. Inputs to the BDT are variables related to the lateral spread of the shower, and isolation energies reconstructed from scalar sums in p_{T} of charged particles and E_{T} sums of photons in a cone with an opening angle $\Delta R = \sqrt{(\Delta\eta)^2 + (\Delta\phi)^2} < 0.3$ around the photon, computed using the particle-flow (PF) algorithm [47, 48].

The η and energy of the supercluster corresponding to the reconstructed photon are also included as input variables in the photon identification BDT. These variables are introduced to explicitly correlate the shower topology and isolation variables with η and p_{T}. Furthermore, during the BDT training, the η and p_{T} background distributions are reweighted to match the distributions in the signal. As a result, for a given requirement on the BDT output, efficiencies for photon identification are almost independent of η and p_{T}, as can be seen in Fig. 1, which provides less model-dependent efficiency corrections for comparison of data and MC expectations at the particle level. A loose selection is applied on the BDT output for photons detected in the barrel region, while a tight selection is applied to endcap photons, with respective mean efficiencies of 95% and 90% for signal photons.

Photon efficiencies in signal samples are corrected for the difference in efficiency between data and simulation as measured with $\mathrm{Z} \to \mathrm{e}^+\mathrm{e}^-$ events, treating electrons as photons by reweighting the electron cluster variable R_9 to that of the R_9 distribution of signal photons. There is good agreement found in the BDT output between data and simulation in $\mathrm{Z} \to \mathrm{e}^+\mathrm{e}^-$ and $\mathrm{Z} \to \mu^+\mu^-\gamma$ events.

4.2 Event classification using an estimator of mass resolution

Measuring differential kinematic distributions implies that events cannot be classified according to the diphoton kinematic BDT used for the inclusive measurement of Ref. [12], as that would create a bias in the result. To improve the performance beyond the simple classification using the R_9 variable in the reference sequential analysis, an event categorization is introduced that is based on the estimated energy resolution.

The photon energy is corrected for the containment of a shower in clustered crystals, the shower

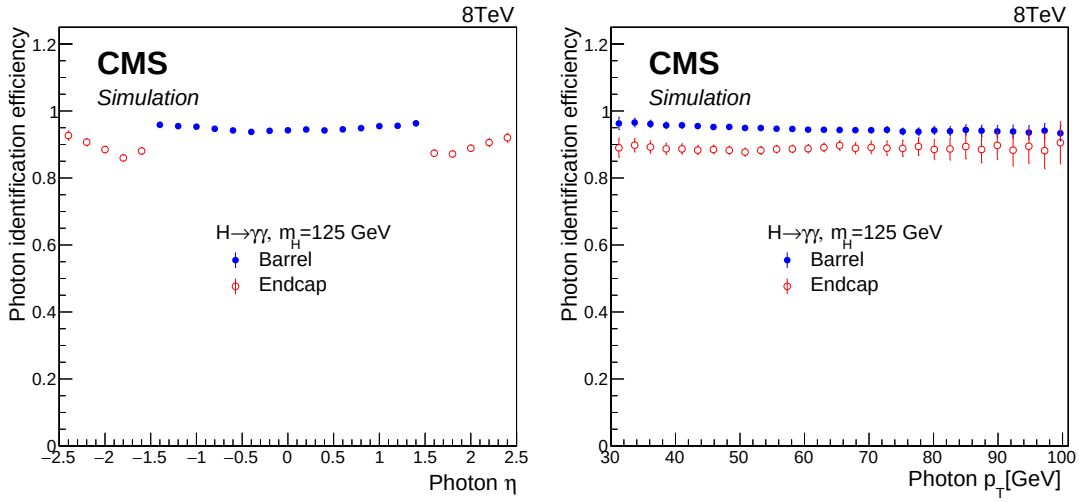

Figure 1: Photon identification efficiencies for a Higgs boson with m_{H} =125 GeV, as a function of photon pseudorapidity (left), and photon transverse momentum (right).

losses for photons that convert in the material upstream of the calorimeter, and the effects of pileup using a multivariate regression technique trained on shower variables and variables related to positions of photons in the detector based on γ+jets simulated events. The energy response to photons is parameterized through an extended form of the Crystal Ball function [49] with a Gaussian core and two power law contributions. The regression provides an estimate of the parameters of the function, and therefore a prediction for the distribution in the ratio of the uncorrected supercluster energy to the true energy. The most probable value of this distribution is taken as the corrected photon energy. The standard deviation of the Gaussian core provides an estimate of the uncertainty in the energy (σ_E).

We define the estimator of the diphoton mass resolution by:

$$\frac{\sigma_m}{m_{\gamma\gamma}} = \frac{1}{2}\sqrt{\left(\frac{\sigma_{E_1}}{E_1}\right)^2 + S_1^2 + \left(\frac{\sigma_{E_2}}{E_2}\right)^2 + S_2^2} \tag{1}$$

where E_1 and E_2 are the corrected energies of the two photons from the regression, σ_{E_1} and σ_{E_2} are the uncertainties in the photon energies, and S_1 and S_2 are smearing terms depending on η, R_9, and E_{T}, determined from $\mathrm{Z} \to \mathrm{e}^+\mathrm{e}^-$ events, needed for the simulation to match the energy resolution in data.

For the typical energy range of photons in this analysis, the relative energy resolution σ_E/E depends on the energy, which in turn introduces a dependence of the mass resolution on the value of $m_{\gamma\gamma}$. Therefore, a categorization based on the diphoton mass resolution introduces a distortion of the background mass spectrum. To obtain a smooth background description, we apply a transformation to the estimator σ_E to decorrelate σ_E/E from the energy.

The decorrelation is performed as a function of photon η, since the energy dependence of σ_E/E varies as a function of η due to changes in the material in front of the ECAL, and because of the inherent properties of the ECAL. In a first step, a transformation is applied to make σ_E/E independent of E and η, the purpose being to ensure that the decorrelation is also independent of the η distribution of the training sample. The decorrelation is performed by forming the cumulative distribution in σ_E as a function of E and η in a γ+jets MC sample that covers a wide range in η and p_{T}. The fully decorrelated variable removes any correlation between σ_E/E and η, and is therefore not suitable for estimating a per-event mass resolution. For this reason, a

second step is introduced to restore the correlation of the energy resolution with photon η in a typical $\mathrm{H} \to \gamma\gamma$ MC sample with $m_{\mathrm{H}} = 125\,\mathrm{GeV}$, and recover thereby a dependence of σ_E on η for the photons of interest. The impact of the particular p_{T} spectrum used for this step is only modest for the correlation of σ_E with η, which is in any case dominated by the material distribution in front of the ECAL and by calorimeter performance. The advantage of such a two-step procedure is that it offers a decorrelated σ_E/E variable that does not depend on the η distribution of the training sample, and it provides the typical energy resolution at a given η of the detector. The final result can be interpreted as an estimator of the average energy resolution at a particular value of η.

The value in the estimator of the mass resolution, after decorrelation, is used to categorize events. The $\sigma_m/m_{\gamma\gamma}$ distribution in $\mathrm{Z} \to \mathrm{e}^+\mathrm{e}^-$ data shown in Fig. 2 indicates good agreement with the MC expectation over the whole range of $\sigma_m/m_{\gamma\gamma}$. The double bump structure corresponds mainly to events where (Fig. 2a) both photons are in the central barrel ($|\eta| < 1.0$, $\sigma_m/m_{\gamma\gamma} < 1\%$), or at least one of the photons is in the outer barrel ($1.00 < |\eta| < 1.44$, $\sigma_m/m_{\gamma\gamma} > 1\%$), and (Fig. 2b) one photon is in the barrel and one in the endcap, both having high values of the R_9 ($\sigma_m/m_{\gamma\gamma} < 1.5\%$), and all the other events ($\sigma_m/m_{\gamma\gamma} > 1.5\%$). The class boundaries in $\sigma_m/m_{\gamma\gamma}$ are optimized in MC samples simultaneously with the photon-identification working points desired to maximize signal significance. The photon identification efficiency is about 95% in each category of $\sigma_m/m_{\gamma\gamma}$. The category with best energy resolution has $\sigma_m/m_{\gamma\gamma} < 0.79\%$, and is composed of events with both selected photons in the central barrel. Both the second ($0.79 < \sigma_m/m_{\gamma\gamma} < 1.28\%$) and third categories ($1.28 < \sigma_m/m_{\gamma\gamma} < 1.83\%$) have at least one photon in the outer barrel or in the endcap. Events with $\sigma_m/m_{\gamma\gamma} > 1.83\%$ do not provide a noticeable improvement in sensitivity and are therefore rejected. Classifying events in these three categories improves the analysis sensitivity by nearly 10%.

It was verified in the simulation that the classification of events according to $\sigma_m/m_{\gamma\gamma}$, after implementing the decorrelation procedure for σ_E, does not produce a distortion of the background distribution in $m_{\gamma\gamma}$.

4.3 Jet identification

Jets are reconstructed using particles identified by the PF algorithm, using the anti-k_{T} [50] algorithm for a distance parameter of 0.5. Jet energy corrections account in particular for pileup, and are obtained from simulation. They are calibrated with in situ measurements using the energy balance studied in dijet and γ/Z+jet events [51]. The jet momentum scale is found to be within 5–10% of the true jet momentum over the whole spectrum and detector acceptance. The jet energy resolution is typically 15% and 8% at 10 and 100 GeV, respectively. Mean resolutions of 10% to 15% are observed in the respective regions of $|\eta| < 0.5$ and $3 < |\eta| < 5$. Jets are selected if they fail the pileup identification criteria [52], and have $p_{\mathrm{T}}^{\mathrm{j}} > 25\,\mathrm{GeV}$. The minimum distance between photons and jets is required to be $\Delta R(\gamma,\mathrm{j}) = \sqrt{\Delta\eta(\gamma,\mathrm{j})^2 + \Delta\phi(\gamma,\mathrm{j})^2} > 0.5$, where $\Delta\eta(\gamma,\mathrm{j})$ and $\Delta\phi(\gamma,\mathrm{j})$ are the pseudorapidity and azimuthal angle differences between photons and jets, to reduce contamination from photons reconstructed as jets.

4.4 Fiducial phase space and observables

The generator-level fiducial volume is chosen to be close to that used in the selection of reconstructed events, and follows previous prescriptions: photons must have $p_{\mathrm{T}}^{\gamma 1}/m_{\gamma\gamma} > 1/3$ and $p_{\mathrm{T}}^{\gamma 2}/m_{\gamma\gamma} > 1/4$, with both photons within $|\eta| < 2.5$. The photons have to be isolated at the generator level, with $\sum_i E_{\mathrm{T}i} < 10\,\mathrm{GeV}$, where i runs over all the other generator-level particles

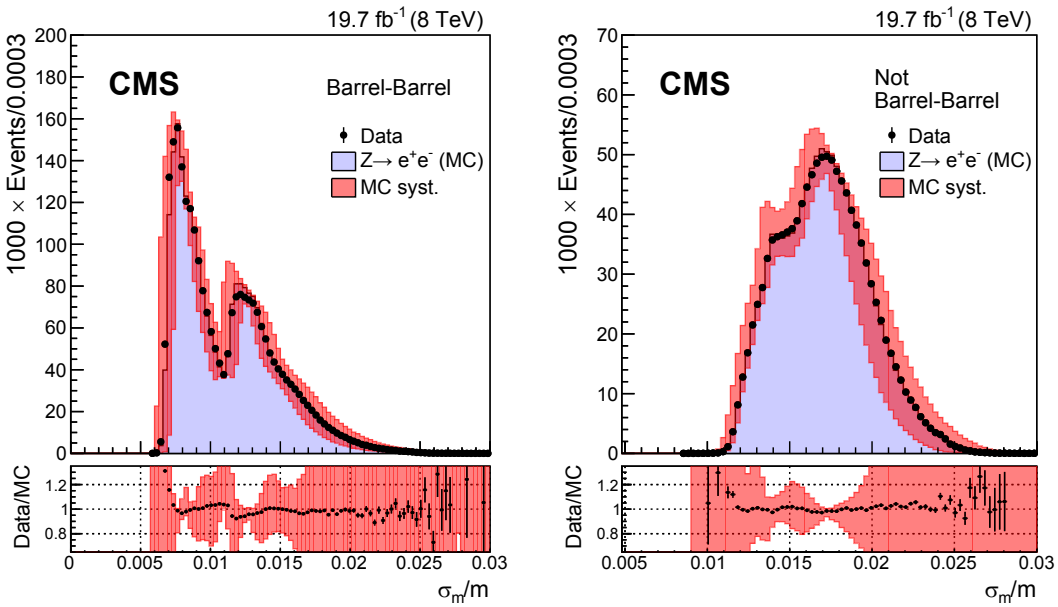

Figure 2: Mass resolution estimator $\sigma_m/m_{\gamma\gamma}$ after the decorrelation procedure, in $Z \to e^+e^-$ events in data (dots) and simulated events (histogram) with their systematic uncertainties (shaded bands) for barrel-barrel events (left), all the other events (right). The ratio of data to MC predictions are shown below each panel, and the error bars on each point represent the statistical uncertainties of the data.

in a cone $\Delta R < 0.4$ around the photons. This selection corresponds to a signal efficiency of 63% in ggH, and almost 60% considering other production mechanisms. We measure the kinematic observables using two-photon criteria, as well as requiring at least one or two jets.

The transverse momentum $p_T^{\gamma\gamma}$ and absolute value of the rapidity $|y^{\gamma\gamma}|$ of the Higgs boson are defined through the inclusive selection. Both $p_T^{\gamma\gamma}$ and $|y^{\gamma\gamma}|$ probe the production mechanism, while the photon helicity angle $\cos\theta^*$ in the Collins–Soper frame [53] of the diphoton system and the difference in azimuth $\Delta\phi^{\gamma\gamma}$ between the two photons are related to properties of the decaying particles.

The number of jets N_{jets}, the transverse momentum p_T^{j1} of the jet with largest (leading) p_T in the event, and the rapidity difference between the Higgs boson and the leading jet $|y^{\gamma\gamma} - y^{j1}|$ are defined after requiring at least one jet with $p_T > 25\,\text{GeV}$ to lie within $|\eta| < 2.5$. The difference in rapidities between the diphoton system and the leading jet provides a sensitive probe of any new contributions to the ggH process.

Requiring at least two jets with $p_T > 25\,\text{GeV}$ and $|\eta| < 4.7$ provides the basis for defining the following observables: the dijet mass m_{jj}, the azimuthal angle difference of the two jets $\Delta\phi^{jj}$, the difference in pseudorapidity $\Delta\eta^{jj}$ between the leading and subleading jet, the Zeppenfeld [54] variable $|\eta^{\gamma\gamma} - (\eta^{j1} + \eta^{j2})/2|$, and the difference in azimuth between the Higgs boson and the dijet system $\Delta\phi^{\gamma\gamma,jj}$. A requirement of $|\eta^j| < 2.5$ is applied in the single-jet selection, as this selection aims to probe primarily ggH process, while the two-jet selection has a requirement $|\eta^j| < 4.7$ since it is oriented toward VBF.

The bin boundaries for each kinematic observable are optimized to achieve similar relative statistical uncertainties in the expected cross section in each bin, namely 60% for each bin in the inclusive observables, 70% in the one-jet observables, and more than 100% in the two-jet observables. The relative statistical uncertainty expected in the fiducial cross section is 30%.

5 Extraction of signal and unfolding of detector effects

The signal yield is extracted by fitting the $m_{\gamma\gamma}$ distribution using a signal model based on simulated events, and a background model determined in the fit to the data. The statistical methodology is similar to Ref. [12], and for each observable the fit is performed simultaneously in all the bins. The reconstructed yields are corrected for detector effects by including the response matrix in the fit.

5.1 Models for signal

Signal models are constructed for each class of $\sigma_m/m_{\gamma\gamma}$ events, and for each production mechanism, from a fit to the simulated $m_{\gamma\gamma}$ distribution, after applying the corrections determined from comparisons of data and simulation for $\mathrm{Z} \to \mathrm{e}^+\mathrm{e}^-$ (also checked with $\mathrm{Z} \to \mu^+\mu^-\gamma$) events, for $m_{\mathrm{H}} = 120, 125$, and 130 GeV. Mass distributions for the best and worst choices of diphoton vertex, corresponding to the highest and lowest scores in the vertexing BDT [12], are fitted separately. Good descriptions of the distributions can be achieved using sums of Gaussian functions, where the means are not required to be identical. As many as four contributing Gaussian functions are used, although in most cases two or three provide an acceptable fit. Models for intermediate values of m_{H} are obtained by linear interpolation of the fitted parameters.

5.2 Statistical methodology

After implementing the above-described selection requirements on photon candidates, a simultaneous binned maximum likelihood fit is performed to the diphoton invariant mass distributions in all the event classes over the range $100 < m_{\gamma\gamma} < 180$ GeV for each differential observable. The test statistic chosen to measure signal and background contributions in data is based on the profile likelihood ratio [55, 56]. Systematic uncertainties are incorporated into the analysis via nuisance parameters and treated according to the frequentist paradigm.

We use the same discrete profiling method to fit the background contribution [57] as used in extracting the main $\mathrm{H} \to \gamma\gamma$ result [12]. The background is evaluated by fitting the $m_{\gamma\gamma}$ distribution in data, without reference to MC simulation. Thus the likelihood to be evaluated in a signal+background hypothesis is

$$\mathcal{L}(\mu_i) = \mathcal{L}(\mathrm{data}|s_i(\mu_i, m_{\gamma\gamma}) + f_i(m_{\gamma\gamma})), \tag{2}$$

where μ_i is the signal strength in the bin i of a differential distribution that is varied in the fit, $s_i(\mu_i, m_{\gamma\gamma})$ represents the model for signal, and $f_i(m_{\gamma\gamma})$ the fitted background functions.

The choice of function used to fit the background in any particular event class is included as a discrete nuisance parameter in the formulation used to extract the result. Exponentials, power-law functions, polynomials in the Bernstein basis, and Laurent polynomials are used to represent $f(m_{\gamma\gamma})$. When fitting a signal+background hypothesis to the data, by minimizing the value of twice the negative logarithm of the likelihood, all functions in these families are tried, with a "penalty" term added to account for the number of free parameters in the fit.

The penalized likelihood function $\widetilde{\mathcal{L}}_f$ for a single fixed background fitting function f is defined through

$$-2\ln\widetilde{\mathcal{L}}_f = -2\ln\mathcal{L}_f + N_f, \tag{3}$$

where $\mathcal{L}_f$ is the "unpenalized" likelihood function, and N_f is the number of free parameters in f. The full set of μ_i, denoted by $\vec{\mu}$, is determined by minimizing the likelihood ratio:

$$L(\vec{\mu}) = -2\ln\frac{\widetilde{\mathcal{L}}(\text{data}|\vec{\mu},\hat{\theta}_{\vec{\mu}},\hat{f}_{\vec{\mu}})}{\widetilde{\mathcal{L}}(\text{data}|\hat{\vec{\mu}},\hat{\theta}_{\hat{\vec{\mu}}},\hat{f}_{\hat{\vec{\mu}}})}, \tag{4}$$

where the numerator represents the maximum of $\widetilde{\mathcal{L}}$ as a function of $\vec{\mu}$, achieved for the best-fit values of the nuisance parameters $\theta_{\vec{\mu}} = \hat{\theta}_{\vec{\mu}}$, and a particular background function $f_{\vec{\mu}} = \hat{f}_{\vec{\mu}}$. The denominator corresponds to the global maximum of $\widetilde{\mathcal{L}}$, where $\vec{\mu} = \hat{\vec{\mu}}$, $\theta_{\vec{\mu}} = \hat{\theta}_{\hat{\vec{\mu}}}$, and $f_{\vec{\mu}} = \hat{f}_{\hat{\vec{\mu}}}$. In each family, the number of degrees of freedom (number of exponentials, number of terms in the series, degree of the polynomial, etc.) is increased until no significant improvement (p value < 0.05 obtained from the F-distribution [58]) occurs in the likelihood between N+1 and N degrees of freedom for the fit to data.

For a given observable, the fit is performed simultaneously over all the bins, and the nuisance parameters are profiled in the fit. The signal mass is also considered a nuisance parameter and profiled for each observable. This choice is made to avoid using the same data twice, first to measure the signal mass, then to measure the kinematic distribution at this mass. As a consequence the differential cross section for each observable is evaluated at slightly different best fit values of the signal mass (see appendix A). As an example, Fig. 3 shows the sum of the fit to the events of the three $\sigma_m/m_{\gamma\gamma}$ classes in the fiducial phase space measurement, under the signal+background hypothesis (S+B), weighted by S/(S+B) separately in each category.

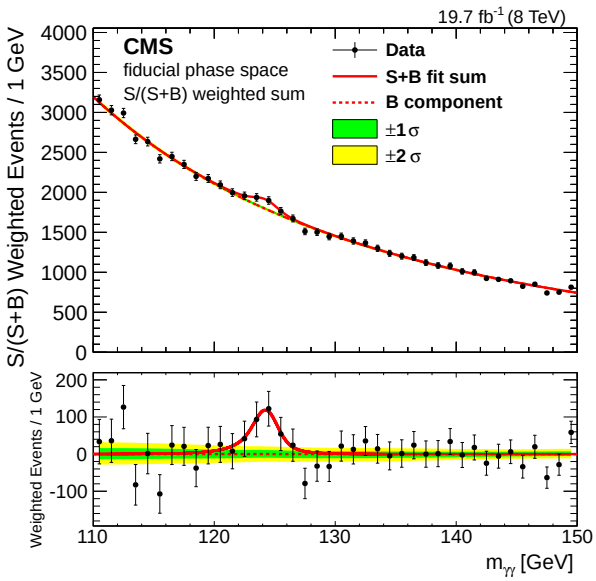

Figure 3: Sum of the signal+background (S+B) model fits to the events of the three $\sigma_m/m_{\gamma\gamma}$ classes in the fiducial phase space measurement, weighted by S/(S+B) separately in each category, together with the data binned as a function of $m_{\gamma\gamma}$. The 1 and 2 standard deviation bands of uncertainty (labeled as 1σ and 2σ) shown for the background component include the uncertainty due to the choice of function and the uncertainty in the fitted parameters. The bottom panel shows the result after subtracting the background component.

The uncertainty on the expected signal strength (ratio of measured to expected yields) of the fiducial cross section is $\sigma_{\hat{\mu}} = 0.32$ for the present analysis, compared with the uncertainty on the expected signal strength obtained with the reference analysis of $\sigma_{\hat{\mu}} = 0.26$ using 8 TeV data.

The reference analysis [12] classifies events using exclusive categories dedicated to measuring signal production in associated mechanisms, while the present analysis is performed inclusively.

5.3 Unfolding detector effects

The measurement is performed simultaneously in all bins, together with the unfolding of the detector effects to the particle level. The same kind of procedure was used to extract the signal strength in untagged and dijet-tagged categories to measure the couplings of the Higgs boson to vector bosons and fermions [12]. This procedure uses asymmetric uncertainties in the full likelihood instead of limiting to Gaussian uncertainties computed with a covariance matrix.

The unfolding of reconstructed distributions is based on models of response matrices K_{ij} in the three $\sigma_m/m_{\gamma\gamma}$ categories for each observable to be measured. The K_{ij} are constructed in the simulation to give the probability of measuring a reconstructed event in bin j, given that it was generated in bin i. The models for contributions of signal are contained in each element of the response matrix, which is mostly diagonal, but can have non-negligible bin-by-bin migration resulting in off-diagonal contributions.

The unfolding is performed using a maximum likelihood technique, adapted to combine the measurement in different categories. Regularization is not used, so as not to shift the best-fit value while artificially decreasing the uncertainties. This leads to minimizing the following conditional log-likelihood expression:

$$\mathcal{F}(\vec{\mu}) = -2\sum_j \log \mathcal{L}\Big(\sum_i K_{ij}\mu_i N_i^{\text{gen}} | N_j^{\text{reco}}\Big) \tag{5}$$

where $\mathcal{L}$ is the log-likelihood expression in Eq. (2), $\mu_i N_i^{\text{gen}}$ is the unknown unfolded particle-level distribution, μ_i is the unknown signal strength modifier at particle level, N_i^{gen} is the particle-level distribution in the simulated kinematic observable, and N_j^{reco} is the number of events in each bin of the measured distribution. The indices i refer to particle-level bins while j refer to reconstructed-level bins in the three $\sigma_m/m_{\gamma\gamma}$ categories.

The expected reconstructed signal at detector level is given by the matrix $J_{ij} = K_{ij}N_i^{\text{gen}}$, where each entry of J_{ij} corresponds therefore to a set of signal models, computed by interpolating the matrix between the generated mass points, weighted by the signal efficiency interpolated at the same mass. The matrix is a function of m_{H}, the model for the generated bin i and the reconstructed bin and category j, as well as all the nuisance parameters. Events falling out of the acceptance are taken into account by forming an extra bin.

The maximum likelihood fit is performed simultaneously for the diphoton background and the signal strength in each generator bin, as described in Section 5.2. The out-of-acceptance bin is left fixed in the fit, because there are only N bins at the reconstructed level, where the detector is able to perform the measurement, and it is therefore not possible to determine an extra unknown at the particle level ($N+1$ unknowns), outside of the detector acceptance. To restore the correct cross section normalization in the fiducial region, the generator distributions for the variables of interest (N_i^{gen} at the fitted mass point m_{H}) are multiplied by the measured set of signal strengths (μ_i).

The enhancement of the statistical uncertainties due to the presence of off-diagonal elements in the response matrix is small for the inclusive observables, while it is non-negligible for the one-jet or two-jet observables. A negative number of events is measured in only one bin of the rapidity difference between the Higgs boson and the leading jet, in the last bin of the dijet mass

distribution, and in two bins of the azimuthal difference between the Higgs boson and the dijet system. In each case, within the uncertainties, the result is compatible with zero.

The model dependence introduced by the unfolding is checked using the following procedure. The same model used for the SM Higgs boson is kept in the unfolding matrix, leaving the expected yield for ggH unchanged. The expected number of signal events arising from associated production mechanisms is altered by 50% in the fit. This change introduces a redistribution of the events in the $\sigma_m/m_{\gamma\gamma}$ categories relative to the nominal analysis. The change in the fiducial cross section is less than 5% of its statistical uncertainty. In general, the impact in each bin of the measured differential distributions can be up to 5% and 10% of the statistical uncertainty in the respective bins of the inclusive and jet observables.

6 Systematic uncertainties

Systematic uncertainties listed in this section are included in the likelihood as nuisance parameters and are profiled during the minimization. The precision of the present measurement is however dominated by statistical uncertainties.

The sources of uncertainty assigned to all events can be summarised as follows. The uncertainty in the integrated luminosity is estimated as described in Ref. [59], and amounts to 2.6% of the signal yield in the data. The uncertainty in the vertex-finding efficiency is taken from the difference observed between data and simulation in $Z \to \mu^+\mu^-$ events, following removal of the muon tracks to mimic a diphoton event. A 1% uncertainty is added to account for the activity from charged-particle tracks in signal, estimated by changing the underlying event tunes in ggH events; another uncertainty of 0.2% accounts for the uncertainty in the $m_{\gamma\gamma}$ distribution of signal events. The uncertainty in the trigger efficiency is extracted from $Z \to e^+e^-$ events using a "tag-and-probe" technique [60]. A rescaling in the R_9 distribution is used to take into account the difference between electrons and photons, for a total uncertainty of 1% assigned for this source.

The following correspond to systematic uncertainties related to individual photons. The uncertainty in the energy scale of photons is assessed using simulated samples in which the amount of tracker material is increased uniformly by 10% in the central barrel, where the material is known with best precision, and 20% out of this region. The resulting uncertainty in the photon energy ranges from 0.03% in the central ECAL barrel up to 0.3% in the outer endcap. Additional uncertainties of 0.015% are due to the modelling of the fraction of scintillation light reaching the photodetector, and from nonuniformities in the radiation-induced loss of transparency of the crystals. A small uncertainty of 0.05% is added to account for modelling of electromagnetic-showers in GEANT4 version 9.4.p03.

Possible differences between MC simulation and data in the extrapolation of shower energies typical of electrons from $Z \to e^+e^-$ decays to those typical of photons from $H \to \gamma\gamma$ decays, have been investigated with $Z \to e^+e^-$ and $W \to e\nu$ data. The effect of differential nonlinearity in the measurement of photon energies has an effect of up to 0.1% on the diphoton mass for $m_{\gamma\gamma} \approx 125\,\text{GeV}$.

The energy scale and resolution in data are measured with electrons from $Z \to e^+e^-$ decays. Systematic uncertainties in the method are estimated as a function of $|\eta|$ and R_9. The uncertainties range from 0.05% for unconverted photons in the central ECAL barrel, to 0.1% for converted photons in the outer endcaps of the ECAL. Finally, there is an overall uncertainty that accounts for possible mismodelling of the $Z \to e^+e^-$ line shape in simulation.

The uncertainties in the BDT discriminant for photon identification and in the estimate of photon energy resolution are discussed together since they are studied in the same way. The dominant underlying cause of the observed differences between data and simulation is the simulation of the energy distribution in the shower. The combined contribution of the uncertainties in these two quantities dominates the experimental contribution to the systematic uncertainty in signal strength. The agreement between data and simulation is examined when photon candidates are electron showers reconstructed as photons in $Z \to e^+e^-$ events, photons in $Z \to \mu^+\mu^-\gamma$ events, and leading photons in preselected diphoton events where $m_{\gamma\gamma} > 160\,\text{GeV}$. A change of ± 0.01 in the value of the photon identification discriminant, together with an uncertainty in the estimated photon energy resolution parameterized, respectively as a rescaling of the resolution estimate by $\pm 5\%$ and $\pm 10\%$ about its nominal value in the barrel and in the endcap, fully cover the differences observed in all three of these data samples.

The uncertainty in the preselection efficiency is taken as the uncertainty in the ratio of data/MC scale factors measured using $Z \to e^+e^-$ events with a tag-and-probe technique.

Jet observables are affected by systematic uncertainties arising from jet identification, jet energy scale, and resolution. For the jet observables, a systematic uncertainty of less than 1% in the impact of the algorithm used to reject jets from pileup is neglected. For jets within $|\eta| < 2.5$, the energy scale uncertainty is $\approx$3% at 30 GeV, and decreases quickly as a function of the increasing jet p_T. The impact of this uncertainty in the cross section is 1–5%, increasing with the number of jets. Dijet observables for forward jets (up to $|\eta| < 4.7$) have the worst energy resolution and a scale uncertainty of $\approx$4.5% at 30 GeV. The impact of these uncertainties on the cross section ranges from 5 to 11%, increasing in kinematical regions of observables where jet η is large. Small contributions from corrections in jet energy resolution have an impact of less than 1% and are neglected.

7 Comparison of data with theory

7.1 Theoretical predictions

The unfolded data are compared with the HRES [42, 43], POWHEG [27–30], POWHEG+MINLO [44], and MADGRAPH5_aMC@NLO [45, 61] MC generators for ggH production.

The HRES parton-level generator corresponds to next-to-next-to-leading order (NNLO) accuracy in perturbative QCD, with next-to-next-to-leading logarithm soft-gluon resummation; HRES v.2.3 assumes finite bottom and top quark masses, using respective values of $m_b = 4.75\,\text{GeV}$ and $m_t = 175\,\text{GeV}$. The renormalization scale μ_R and factorization scale μ_F are set to $m_H = 125\,\text{GeV}$, while the resummation scale is set to $m_H/2$. The MSTW2008NNLO [62] PDF is used for the central value, and its 68% confidence level eigenvectors for computing the uncertainty (following the LHAPDF [63] recipe). The dependence on scale is evaluated by changing independently both the renormalization and factorization scale up and down by a factor of two around the central value m_H, and not considering simultaneous changes such as $\mu_R = m_H/2$ and $\mu_F = 2m_H$. Because HRES cannot be interfaced to a parton-shower program, no isolation is applied at the partonic level. A nonperturbative correction must be applied to the distributions to correct for the efficiency loss due to isolation requirements in the presence of parton shower and underlying event. The nonperturbative correction is evaluated from the mean of the isolation efficiencies computed with POWHEG and MADGRAPH5_aMC@NLO (as described below), estimated to be 3.1% (up to 5% in some bins). The uncertainty is taken as half of the envelope, which is between 0.5% to 5%, depending on the kinematical region.

The POWHEG parton-level generator implements NLO calculations [27] interfaced to parton shower programs. Samples of events with a Higgs boson with $m_{\mathrm{H}} = 125\,\mathrm{GeV}$ produced via ggH, assuming an infinite top quark mass, are generated and hadronized with PYTHIA 6.4. A sample of events with a Higgs boson produced in association with just a single jet, called POWHEG HJ, is also generated with POWHEG+MINLO [44]. This sample has NLO accuracy for 0-jet and 1-jet production, while it is only leading-order (LO) for 2-jet final states. Both samples set the damping factor *hfact* in POWHEG at 100 GeV to reproduce the predicted p_{T} distribution of the Higgs boson from HqT [35, 36]. This factor minimizes emission of extra jets beyond those in the matrix element in the limit of large p_{T}, and enhances contribution from the POWHEG Sudakov form factor as p_{T} approaches 0. The CT10 PDF and PYTHIA 6 tune Z2* are used in the calculation. Theoretical uncertainties are computed in the same way as described for HRES.

The MADGRAPH5_aMC@NLO matrix element generator is capable of generating LO and NLO processes [61]. The ggH process is generated using the NLO Higgs characterization model [64], with effective coupling of the Higgs boson to gluons in the infinite top quark mass limit. Gluon fusion is generated with 0, 1, or 2 additional jets at NLO in the Born matrix element, and combined using FxFx merging [65]. Samples are generated using the CT10 PDF, and showered using PYTHIA 8.185 [66] with the 4C tune [67]. A nominal merging scale of 30 GeV is used for the additional jet multiplicities. The effect of changing the merging scale from 20 to 60 GeV is very small compared to uncertainties in scale and in the choice of PDF. Uncertainties from renormalization and factorization scales are evaluated in the same way as with HRES and POWHEG.

Theoretical predictions for associated production mechanisms are computed with the following generators. POWHEG interfaced with PYTHIA 6 is used for VBF, while standalone PYTHIA 6 is used for VH and $\mathrm{t\bar{t}H}$. In the following, the notation XH refers to the sum of VBF, VH and $\mathrm{t\bar{t}H}$ predictions for these generators. Each of the ggH predictions for HRES, POWHEG, MADGRAPH5_aMC@NLO, POWHEG+MINLO, and XH processes are normalized to the total cross sections from Ref. [20].

Along with the SM predictions, the following alternative models are considered. Spin 2^+_m minimal model (graviton-like) initiated through two production mechanisms: ggH and $\mathrm{q\bar{q}}$ annihiliation, based on the JHUGEN generator [21, 68] and normalized to the total SM cross section. The main changes relative to the SM are expected in the inclusive Collins-Soper $\cos\theta^*$ angular distribution in the $\gamma\gamma$ rest frame, which provides maximum information on the spin of the $\gamma\gamma$ system. The two spin-2 samples are compared to the data in the $\cos\theta^*$ observable. Anomalous couplings parametrized with the O_W dimension-6 operator in linearly realized effective field theory [69] are also considered, and implemented through the Universal FeynRules Output [70] in MADGRAPH 5. The O_W operator is related to the anomalous triple gauge coupling parameter Δg_1^Z [71]. The values of the Wilson coefficients are $F_W = -5 \times 10^{-5}\,\mathrm{GeV}^{-4}$ and $F_W = +5 \times 10^{-5}\,\mathrm{GeV}^{-4}$, both corresponding to $\Delta g_1^Z = 0.21$, a value approximately five times the size of the limits set by LHC diboson measurements [72–75]. Both values modify the kinematic distributions of the Higgs boson in the VBF process toward larger p_{T}, and the $F_W = -5 \times 10^{-5}\,\mathrm{GeV}^{-4}$ value also increases the VBF cross section by approximately a factor of 3.

All the predictions are generated at $m_{\mathrm{H}} = 125\,\mathrm{GeV}$. For each observable, a correction factor is applied in each bin of the differential cross section to correct for the mass difference of the generated sample relative to the measured m_{H} in data. The correction is computed with POWHEG+PYTHIA 8 for both the ggH and VBF processes, and with PYTHIA 6 for VH and $\mathrm{t\bar{t}H}$ processes. It amounts to less than 1% for all bins, and integrates to a 0.8% effect in the fiducial

cross section.

7.2 Results

The fiducial cross section, inclusive in the number of jets, is measured to be:

$$\sigma_{\text{obs}} = 32^{+10}_{-10}\,(\text{stat})^{+3}_{-3}\,(\text{syst})\,\text{fb},$$

where the uncertainties reflect statistical and systematic contributions added in quadrature. This can be compared with the following SM predictions:

$$\begin{aligned}\sigma_{\text{HRES+XH}} &= 31^{+4}_{-3}\,\text{fb},\\ \sigma_{\text{POWHEG+XH}} &= 32^{+6}_{-5}\,\text{fb},\\ \sigma_{\text{MADGRAPH5_aMC@NLO+XH}} &= 30^{+6}_{-5}\,\text{fb}.\end{aligned}$$

Uncertainties in the predicted cross sections include contributions from renormalization and factorization scales, choice of PDF and branching fraction. The HRES also includes uncertainties from nonperturbative corrections.

The observed fiducial cross section agrees with the predicted values. The measurement precision is dominated by statistical uncertainties. The relative systematic uncertainty of 9% is almost negligible relative to the statistical uncertainty of 30%. The experimental uncertainty is larger than the theoretical one by a factor up to about two. The ratio of the measured cross section to the predictions for POWHEG+XH is in good agreement with the signal strength observed in Ref. [12].

The measured differential cross sections observed in data, given for each bin by $\mu_i N_i^{\text{gen}}$, are compared with predictions for inclusive production in Fig. 4, and for jet observables in Figs. 5 and 6. The total theoretical uncertainty included in these comparisons is computed by adding in an uncorrelated way the uncertainties in the choice of PDF, renormalization and factorization scale, and the branching fraction. The uncertainties in the ggH mechanism, PDF choice, and the renormalization and factorization scales are computed with HRES, POWHEG, POWHEG+MINLO and MADGRAPH5_aMC@NLO, as described above, while the branching fraction for all production mechanisms, as well as the scale and PDF for the associated production mechanisms are taken from Ref. [20]. Distributions for inclusive observables computed with HRES, POWHEG, and MADGRAPH5_aMC@NLO, and jet-related observables computed with POWHEG, POWHEG+MINLO and MADGRAPH5_aMC@NLO, including latest higher-order corrections, are compatible within their uncertainties, and also compatible with the data.

Figure 4 (upper left) shows the p_{T} distribution of the Higgs boson, which is sensitive to higher-order corrections in perturbative QCD. Figure 4 (upper right) shows the absolute rapidity distribution of the Higgs boson, which is sensitive to the proton PDF, as well as to the production mechanism. Figure 4 (lower left) shows the $\Delta\phi^{\gamma\gamma}$ distribution. Figure 4 (lower right) displays the $\cos\theta^*$ distribution, which is sensitive to the spin of the Higgs boson. The two spin-2 samples indicate deviations relative to the SM predictions. As in the case of Ref. [12], data do not have sufficient sensitivity to discriminate between spin-2 and spin-0 hypotheses.

Figure 5 (upper left) shows the p_{T} distribution for the leading jet, which is sensitive to higher-order QCD effects, and Fig. 5 (upper right) shows the rapidity difference between the Higgs boson and the leading jet. The distribution in the number of jets is displayed in Fig. 5 (lower left). The last bin gives the cross section for signal events with at least three jets. The distribution in the dijet mass shown in Fig. 5 (lower right) is sensitive to the VBF production mechanism, and

especially to a possible anomalous electroweak production in the tail of the distribution. Large contributions from new processes modifying triple gauge couplings would be detected as excesses either in $p_{\mathrm{T}}^{\gamma\gamma}$, $p_{\mathrm{T}}^{\mathrm{j1}}$ or in m_{jj} distributions. The distributions in data are compatible with expectations from the SM within their uncertainties. Figure 6 (upper left) shows the difference in azimuthal angle $\Delta\phi^{\mathrm{jj}}$ between the two jets of highest p_{T}. Figures 6 (upper right), 6 (lower left), and 6 (lower right) show, respectively, the distribution of the rapidity difference between the two jets, the Zeppenfeld variable, and the azimuthal difference between the Higgs boson and the dijet system. These angular variables are sensitive to the VBF topology, and large contributions from anomalous couplings are not observed in data. The distributions in data are compatible with SM predictions within their statistical, systematic, and theoretical uncertainties.

8 Summary

A measurement was carried out of differential cross sections as a function of kinematic observables in the $\mathrm{H} \to \gamma\gamma$ decay channel, using data collected by the CMS experiment at $\sqrt{s} = 8\,\mathrm{TeV}$, corresponding to an integrated luminosity of $19.7\,\mathrm{fb}^{-1}$. The measurement was performed for events with two isolated photons in the kinematic range $p_{\mathrm{T}}^{\gamma 1}/m_{\gamma\gamma} > 1/3$ and $p_{\mathrm{T}}^{\gamma 2}/m_{\gamma\gamma} > 1/4$, with photon pseudorapidities within $|\eta| < 2.5$. Photon identification was chosen to reduce the dependence of the measurement on the kinematics of the signal. Event classification relied on an estimator of diphoton mass resolution. The signal extraction and the unfolding of experimental resolution were performed simultaneously in all bins of the chosen observables. In this kinematic range, the fiducial cross section was measured to be $32 \pm 10\,\mathrm{fb}$.

The differential cross section of the Higgs boson was measured, inclusively in the number of jets, as a function of its transverse momentum $p_{\mathrm{T}}^{\gamma\gamma}$, its rapidity $|y^{\gamma\gamma}|$, the Collins-Soper angular variable $\cos\theta^*$, the difference in azimuthal angle between the two photons $\Delta\phi^{\gamma\gamma}$, and the number of associated jets N_{jets}. The transverse momentum of the leading jet $p_{\mathrm{T}}^{\mathrm{j1}}$, and the difference in rapidity between the Higgs boson and the leading jet $|y^{\gamma\gamma} - y^{\mathrm{j1}}|$ were determined in events with at least one accompanying jet. In events with at least two jets, measurements were made of the dijet mass m_{jj}, the azimuth between the two jets $\Delta\phi^{\mathrm{jj}}$, the pseudorapidity difference between the two jets $\Delta\eta^{\mathrm{jj}}$, the Zeppenfeld variable $|\eta^{\gamma\gamma} - (\eta^{\mathrm{j1}} + \eta^{\mathrm{j2}})/2|$, and the azimuthal angle between the Higgs boson and the dijet system $\Delta\phi^{\gamma\gamma,\mathrm{jj}}$. The differential cross sections were compared with several SM and beyond SM calculations, and found to be compatible with the SM predictions within statistical, systematic, and theoretical uncertainties.

Acknowledgments

We congratulate our colleagues in the CERN accelerator departments for the excellent performance of the LHC and thank the technical and administrative staffs at CERN and at other CMS institutes for their contributions to the success of the CMS effort. In addition, we gratefully acknowledge the computing centers and personnel of the Worldwide LHC Computing Grid for delivering so effectively the computing infrastructure essential to our analyses. Finally, we acknowledge the enduring support for the construction and operation of the LHC and the CMS detector provided by the following funding agencies: the Austrian Federal Ministry of Science, Research and Economy and the Austrian Science Fund; the Belgian Fonds de la Recherche Scientifique, and Fonds voor Wetenschappelijk Onderzoek; the Brazilian Funding Agencies (CNPq, CAPES, FAPERJ, and FAPESP); the Bulgarian Ministry of Education and

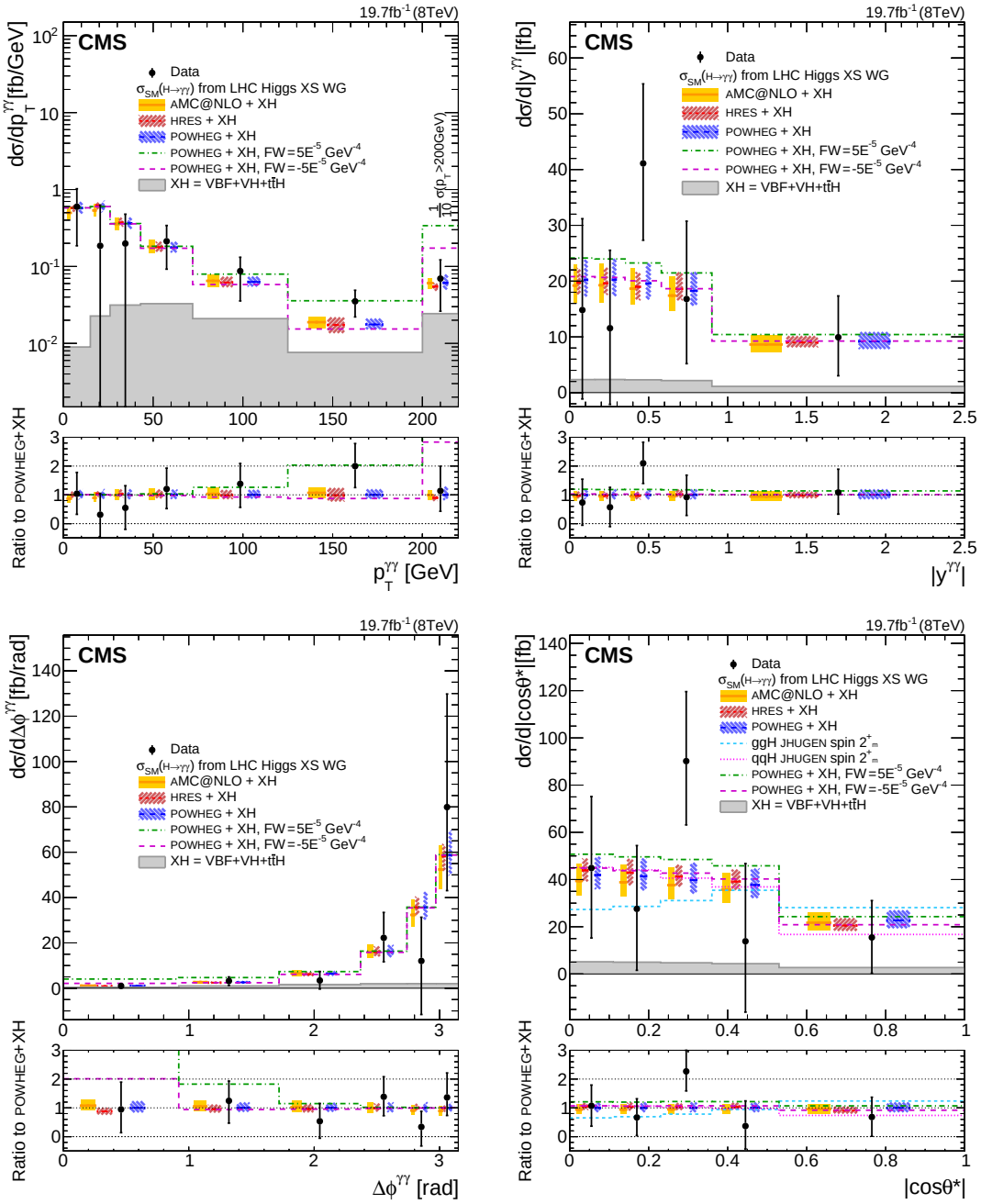

Figure 4: The H $\rightarrow \gamma\gamma$ differential cross section for inclusive events as a function of (upper left) $p_T^{\gamma\gamma}$, (upper right) $|y^{\gamma\gamma}|$, (lower left) $\Delta\phi^{\gamma\gamma}$, and (lower right) $|\cos\theta^*|$. All the SM contributions are normalized to their cross section from Ref. [20]. Theoretical uncertainties in the renormalization and factorization scales, PDF, and branching fraction are added in quadrature. The error bars on data points reflect both statistical and systematic uncertainties. The last bin of $p_T^{\gamma\gamma}$ distribution sums the events above 200 GeV. For each graph, the bottom panel shows the ratio of data to theoretical predictions from POWHEG generator.

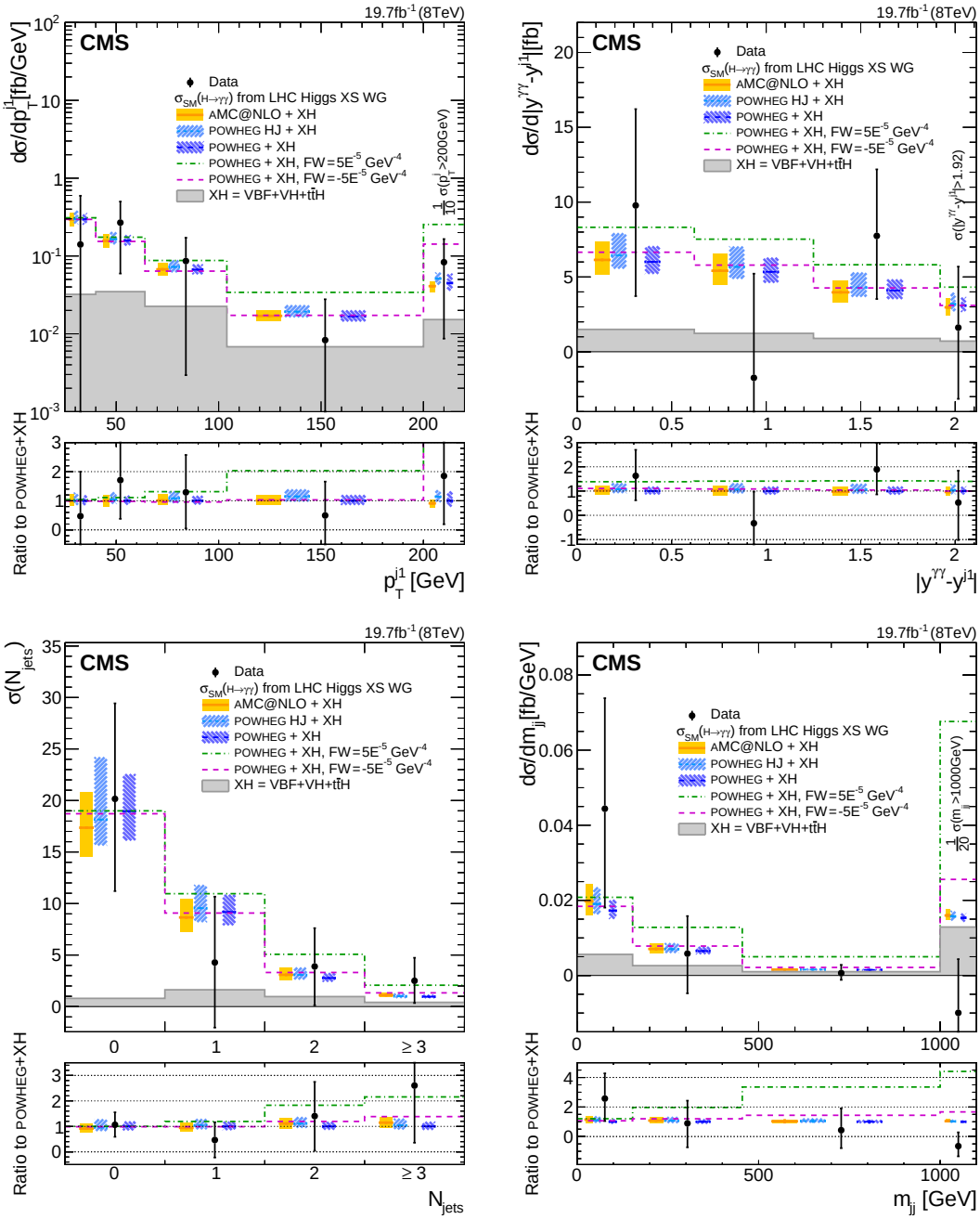

Figure 5: The H $\rightarrow \gamma\gamma$ differential cross section for H+jets events as a function of (upper left) $p_{\mathrm{T}}^{\mathrm{j1}}$, (upper right) $|y^{\gamma\gamma} - y^{\mathrm{j1}}|$, (lower left) N_{jets}, with jets within $|\eta| < 2.5$, and (lower right) m_{jj} with jets within $|\eta| < 4.7$. All the SM contributions are normalized to their cross section from Ref. [20]. Theoretical uncertainties in the renormalization and factorization scales, PDF, and branching fraction are added in quadrature. The error bars on data points reflect both statistical and systematic uncertainties. In each distribution, the last bin corresponds to the sum over the events beyond the bins shown in the figure. For each graph, the bottom panel shows the ratio of data to theoretical predictions from POWHEG generator.

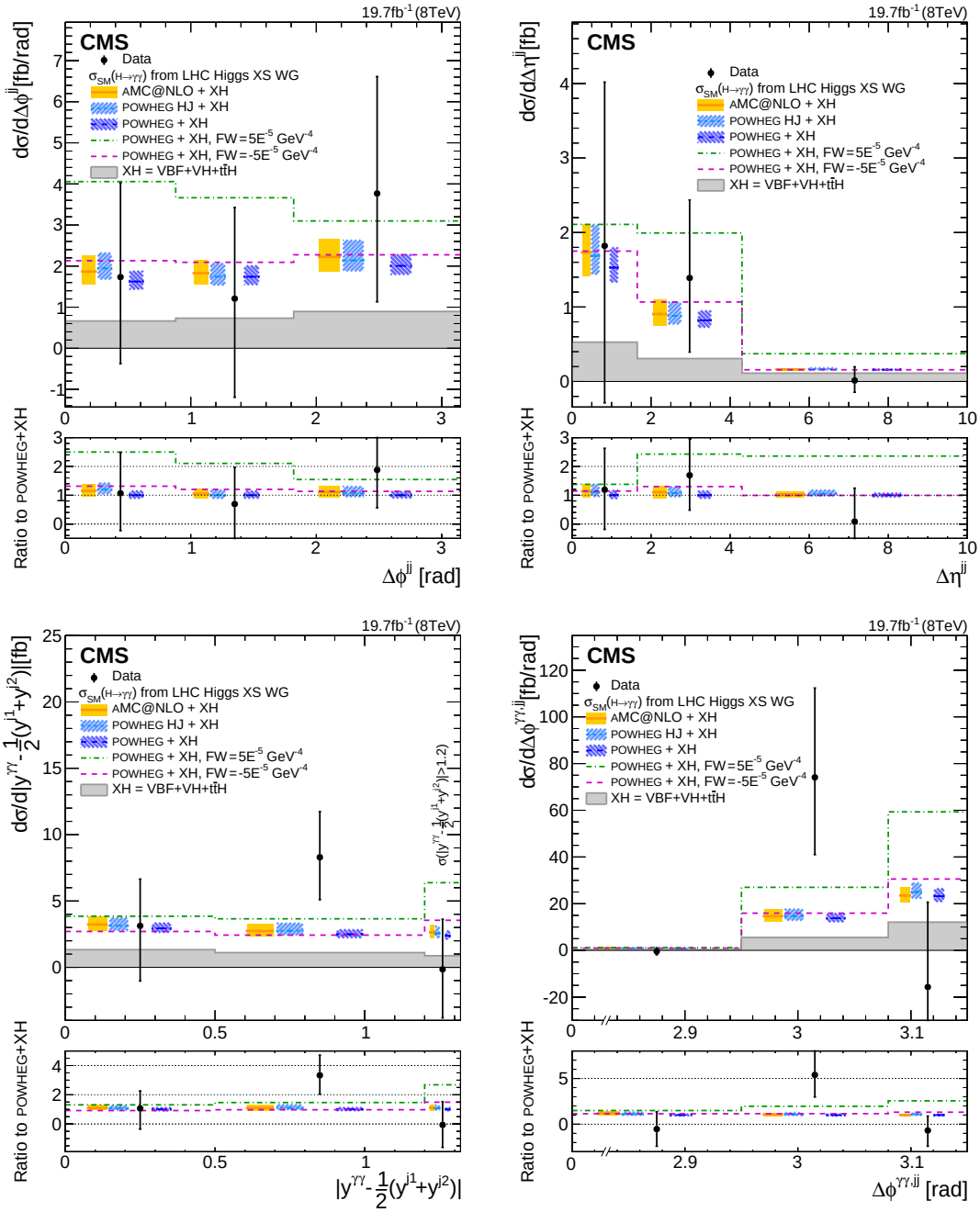

Figure 6: The H $\rightarrow \gamma\gamma$ differential cross section for H+2 jets events, with jets within $|\eta| < 4.7$, as a function of (upper left) $\Delta\phi^{jj}$, (upper right) $\Delta\eta^{jj}$, (lower left) Zeppenfeld variable, and (lower right) $\Delta\phi^{\gamma\gamma,jj}$. All the SM contributions are normalized to their cross section from Ref. [20]. Theoretical uncertainties in the renormalization and factorization scales, PDF, and branching fraction are added in quadrature. The error bars on data points reflect both statistical and systematic uncertainties. In the Zeppenfeld distribution, the last bin sums the events with values above 1.2. For each graph, the bottom panel shows the ratio of data to theoretical predictions from POWHEG generator.

Science; CERN; the Chinese Academy of Sciences, Ministry of Science and Technology, and National Natural Science Foundation of China; the Colombian Funding Agency (COLCIENCIAS); the Croatian Ministry of Science, Education and Sport, and the Croatian Science Foundation; the Research Promotion Foundation, Cyprus; the Ministry of Education and Research, Estonian Research Council via IUT23-4 and IUT23-6 and European Regional Development Fund, Estonia; the Academy of Finland, Finnish Ministry of Education and Culture, and Helsinki Institute of Physics; the Institut National de Physique Nucléaire et de Physique des Particules / CNRS, and Commissariat à l'Énergie Atomique et aux Énergies Alternatives / CEA, France; the Bundesministerium für Bildung und Forschung, Deutsche Forschungsgemeinschaft, and Helmholtz-Gemeinschaft Deutscher Forschungszentren, Germany; the General Secretariat for Research and Technology, Greece; the National Scientific Research Foundation, and National Innovation Office, Hungary; the Department of Atomic Energy and the Department of Science and Technology, India; the Institute for Studies in Theoretical Physics and Mathematics, Iran; the Science Foundation, Ireland; the Istituto Nazionale di Fisica Nucleare, Italy; the Ministry of Science, ICT and Future Planning, and National Research Foundation (NRF), Republic of Korea; the Lithuanian Academy of Sciences; the Ministry of Education, and University of Malaya (Malaysia); the Mexican Funding Agencies (CINVESTAV, CONACYT, SEP, and UASLP-FAI); the Ministry of Business, Innovation and Employment, New Zealand; the Pakistan Atomic Energy Commission; the Ministry of Science and Higher Education and the National Science Centre, Poland; the Fundação para a Ciência e a Tecnologia, Portugal; JINR, Dubna; the Ministry of Education and Science of the Russian Federation, the Federal Agency of Atomic Energy of the Russian Federation, Russian Academy of Sciences, and the Russian Foundation for Basic Research; the Ministry of Education, Science and Technological Development of Serbia; the Secretaría de Estado de Investigación, Desarrollo e Innovación and Programa Consolider-Ingenio 2010, Spain; the Swiss Funding Agencies (ETH Board, ETH Zurich, PSI, SNF, UniZH, Canton Zurich, and SER); the Ministry of Science and Technology, Taipei; the Thailand Center of Excellence in Physics, the Institute for the Promotion of Teaching Science and Technology of Thailand, Special Task Force for Activating Research and the National Science and Technology Development Agency of Thailand; the Scientific and Technical Research Council of Turkey, and Turkish Atomic Energy Authority; the National Academy of Sciences of Ukraine, and State Fund for Fundamental Researches, Ukraine; the Science and Technology Facilities Council, UK; the US Department of Energy, and the US National Science Foundation.

Individuals have received support from the Marie-Curie program and the European Research Council and EPLANET (European Union); the Leventis Foundation; the A. P. Sloan Foundation; the Alexander von Humboldt Foundation; the Belgian Federal Science Policy Office; the Fonds pour la Formation à la Recherche dans l'Industrie et dans l'Agriculture (FRIA-Belgium); the Agentschap voor Innovatie door Wetenschap en Technologie (IWT-Belgium); the Ministry of Education, Youth and Sports (MEYS) of the Czech Republic; the Council of Science and Industrial Research, India; the HOMING PLUS program of the Foundation for Polish Science, cofinanced from European Union, Regional Development Fund; the OPUS program of the National Science Center (Poland); the Compagnia di San Paolo (Torino); the Consorzio per la Fisica (Trieste); MIUR project 20108T4XTM (Italy); the Thalis and Aristeia programs cofinanced by EU-ESF and the Greek NSRF; the National Priorities Research Program by Qatar National Research Fund; the Rachadapisek Sompot Fund for Postdoctoral Fellowship, Chulalongkorn University (Thailand); and the Welch Foundation, contract C-1845.

References

[1] ATLAS Collaboration, "Observation of a new particle in the search for the Standard

Model Higgs boson with the ATLAS detector at the LHC", *Phys. Lett. B* **716** (2012) 1, doi:10.1016/j.physletb.2012.08.020, arXiv:1207.7214.

[2] CMS Collaboration, "Observation of a new boson at a mass of 125 GeV with the CMS experiment at the LHC", *Phys. Lett. B* **716** (2012) 30, doi:10.1016/j.physletb.2012.08.021.

[3] CMS Collaboration, "Observation of a new boson with mass near 125 GeV in pp collisions at $\sqrt{s}$ = 7 and 8 TeV", *JHEP* **06** (2013) 081, doi:10.1007/JHEP06(2013)081, arXiv:1303.4571.

[4] S. L. Glashow, "Partial-symmetries of weak interactions", *Nucl. Phys.* **22** (1961) 579, doi:10.1016/0029-5582(61)90469-2.

[5] S. Weinberg, "A Model of Leptons", *Phys. Rev. Lett.* **19** (1967) 1264, doi:10.1103/PhysRevLett.19.1264.

[6] A. Salam, "Weak and electromagnetic interactions", in *Elementary particle physics: relativistic groups and analyticity*, N. Svartholm, ed., p. 367. Almqvist & Wiskell, 1968. Proceedings of the eighth Nobel symposium.

[7] F. Englert and R. Brout, "Broken Symmetry and the Mass of Gauge Vector Mesons", *Phys. Rev. Lett.* **13** (1964) 321, doi:10.1103/PhysRevLett.13.321.

[8] P. W. Higgs, "Broken Symmetries and the Masses of Gauge Bosons", *Phys. Rev. Lett.* **13** (1964) 508, doi:10.1103/PhysRevLett.13.508.

[9] G. S. Guralnik, C. R. Hagen, and T. W. B. Kibble, "Global Conservation Laws and Massless Particles", *Phys. Rev. Lett.* **13** (1964) 585, doi:10.1103/PhysRevLett.13.585.

[10] P. W. Higgs, "Spontaneous Symmetry Breakdown without Massless Bosons", *Phys. Rev.* **145** (1966) 1156, doi:10.1103/PhysRev.145.1156.

[11] T. W. B. Kibble, "Symmetry Breaking in Non-Abelian Gauge Theories", *Phys. Rev.* **155** (1967) 1554, doi:10.1103/PhysRev.155.1554.

[12] CMS Collaboration, "Observation of the diphoton decay of the Higgs boson and measurement of its properties", *Eur. Phys. J. C* **74** (2014) 3076, doi:10.1140/epjc/s10052-014-3076-z, arXiv:1407.0558.

[13] ATLAS Collaboration, "Measurement of Higgs boson production in the diphoton decay channel in pp collisions at center-of-mass energies of 7 and 8 TeV with the ATLAS detector", *Phys. Rev. D* **90** (2014) 112015, doi:10.1103/PhysRevD.90.112015, arXiv:1408.7084.

[14] CMS Collaboration, "Precise determination of the mass of the Higgs boson and tests of compatibility of its couplings with the standard model predictions using proton collisions at 7 and 8 TeV", *Eur. Phys. J. C* **75** (2015) 212, doi:10.1140/epjc/s10052-015-3351-7, arXiv:1412.8662.

[15] ATLAS Collaboration, "Evidence for the spin-0 nature of the Higgs boson using ATLAS data", *Phys. Lett. B* **726** (2013) 120, doi:10.1016/j.physletb.2013.08.026, arXiv:1307.1432.

[16] CMS Collaboration, "Constraints on the spin-parity and anomalous HVV couplings of the Higgs boson in proton collisions at 7 and 8 TeV", *Phys. Rev. D* **92** (2015), no. 1, 012004, doi:10.1103/PhysRevD.92.012004, arXiv:1411.3441.

[17] ATLAS Collaboration, "Measurements of fiducial and differential cross sections for Higgs boson production in the diphoton decay channel at $\sqrt{s} = 8$ TeV with ATLAS", *JHEP* **09** (2014) 112, doi:10.1007/JHEP09(2014)112, arXiv:1407.4222.

[18] ATLAS Collaboration, "Fiducial and differential cross sections of Higgs boson production measured in the four-lepton decay channel in pp collisions at $\sqrt{s} = 8$ TeV with the ATLAS detector", *Phys. Lett. B* **738** (2014) 234, doi:10.1016/j.physletb.2014.09.054, arXiv:1408.3226.

[19] ATLAS Collaboration, "Measurements of the Total and Differential Higgs Boson Production Cross Sections Combining the $H \to \gamma\gamma$ and $H \to ZZ^* \to 4\ell$ Decay Channels at $\sqrt{s} = 8$ TeV with the ATLAS Detector", (2015). arXiv:1504.05833. Submitted to PRL.

[20] LHC Higgs Cross Section Working Group, "Handbook of LHC Higgs cross sections: 3. Higgs Properties", CERN Report CERN-2013-004, 2013. doi:10.5170/CERN-2013-004, arXiv:1307.1347.

[21] Y. Gao et al., "Spin determination of single-produced resonances at hadron colliders", *Phys. Rev. D* **81** (2010) 075022, doi:10.1103/PhysRevD.81.075022, arXiv:1001.3396.

[22] C. Grojean, E. Salvioni, M. Schlaffer, and A. Weiler, "Very boosted Higgs in gluon fusion", *JHEP* **05** (2014) 022, doi:10.1007/JHEP05(2014)022, arXiv:1312.3317.

[23] CMS Collaboration, "The CMS experiment at the CERN LHC", *JINST* **3** (2008) S08004, doi:10.1088/1748-0221/3/08/S08004.

[24] CMS Collaboration, "Energy calibration and resolution of the CMS electromagnetic calorimeter in pp collisions at $\sqrt{s}$ = 7 TeV", *JINST* **8** (2013) P09009, doi:10.1088/1748-0221/8/09/P09009, arXiv:1306.2016.

[25] CMS Collaboration, "Performance of photon reconstruction and identification with the CMS detector in proton-proton collisions at $\sqrt{s}$ = 8 TeV", *JINST* **10** (2015) P08010, doi:10.1088/1748-0221/10/08/P08010, arXiv:1502.02702.

[26] GEANT4 Collaboration, "GEANT4—a simulation toolkit", *Nucl. Instrum. Meth. A* **506** (2003) 250, doi:10.1016/S0168-9002(03)01368-8.

[27] P. Nason, "A new method for combining NLO QCD with shower Monte Carlo algorithms", *JHEP* **11** (2004) 040, doi:10.1088/1126-6708/2004/11/040, arXiv:hep-ph/0409146.

[28] S. Frixione, P. Nason, and C. Oleari, "Matching NLO QCD computations with parton shower simulations: the POWHEG method", *JHEP* **11** (2007) 070, doi:10.1088/1126-6708/2007/11/070, arXiv:0709.2092.

[29] S. Alioli, P. Nason, C. Oleari, and E. Re, "A general framework for implementing NLO calculations in shower Monte Carlo programs: the POWHEG BOX", *JHEP* **06** (2010) 043, doi:10.1007/JHEP06(2010)043, arXiv:1002.2581.

[30] S. Alioli, P. Nason, C. Oleari, and E. Re, "NLO Higgs boson production via gluon fusion matched with shower in POWHEG", *JHEP* **04** (2009) 002, doi:10.1088/1126-6708/2009/04/002, arXiv:0812.0578.

[31] P. Nason and C. Oleari, "NLO Higgs boson production via vector-boson fusion matched with shower in POWHEG", *JHEP* **02** (2010) 037, doi:10.1007/JHEP02(2010)037, arXiv:0911.5299.

[32] T. Sjöstrand, S. Mrenna, and P. Z. Skands, "PYTHIA 6.4 physics and manual", *JHEP* **05** (2006) 026, doi:10.1088/1126-6708/2006/05/026, arXiv:hep-ph/0603175.

[33] H.-L. Lai et al., "New parton distributions for collider physics", *Phys. Rev. D* **82** (2010) 074024, doi:10.1103/PhysRevD.82.074024, arXiv:1007.2241.

[34] LHC Higgs Cross Section Working Group, "Handbook of LHC Higgs cross sections: 2. Differential Distributions", CERN Report CERN-2012-002, 2012. doi:10.5170/CERN-2012-002, arXiv:1201.3084.

[35] G. Bozzi, S. Catani, D. de Florian, and M. Grazzini, "Transverse-momentum resummation and the spectrum of the Higgs boson at the LHC", *Nucl. Phys. B* **737** (2006) 73, doi:10.1016/j.nuclphysb.2005.12.022, arXiv:hep-ph/0508068.

[36] D. de Florian, G. Ferrera, M. Grazzini, and D. Tommasini, "Transverse-momentum resummation: Higgs boson production at the Tevatron and the LHC", *JHEP* **11** (2011) 064, doi:10.1007/JHEP11(2011)064, arXiv:1109.2109.

[37] R. Field, "Early LHC Underlying Event Data - Findings and Surprises", in *22nd Hadron Collider Physics Symposium (HCP 2010)*, W. Trischuk, ed. Toronto, 2010. arXiv:1010.3558.

[38] J. Pumplin et al., "New generation of parton distributions with uncertainties from global QCD analysis", *JHEP* **07** (2002) 012, doi:10.1088/1126-6708/2002/07/012, arXiv:hep-ph/0201195.

[39] L. J. Dixon and M. S. Siu, "Resonance-Continuum Interference in the Diphoton Higgs Signal at the LHC", *Phys. Rev. Lett.* **90** (2003) 252001, doi:10.1103/PhysRevLett.90.252001, arXiv:hep-ph/0302233.

[40] E. Re, "NLO corrections merged with parton showers for Z+2 jets production using the POWHEG method", *JHEP* **10** (2012) 031, doi:10.1007/JHEP10(2012)031, arXiv:1204.5433.

[41] T. Gleisberg et al., "Event generation with SHERPA 1.1", *JHEP* **02** (2009) 007, doi:10.1088/1126-6708/2009/02/007, arXiv:0811.4622.

[42] D. de Florian, G. Ferrera, M. Grazzini, and D. Tommasini, "Higgs boson production at the LHC: transverse momentum resummation effects in the $H \to \gamma\gamma$, $H \to WW \to l\nu l\nu$ and $H \to ZZ \to 4l$ decay modes", *JHEP* **06** (2012) 132, doi:10.1007/JHEP06(2012)132, arXiv:1203.6321.

[43] M. Grazzini and H. Sargsyan, "Heavy-quark mass effects in Higgs boson production at the LHC", *JHEP* **09** (2013) 129, doi:10.1007/JHEP09(2013)129, arXiv:1306.4581.

[44] K. Hamilton, P. Nason, and G. Zanderighi, "MINLO: multi-scale improved NLO", *JHEP* **10** (2012) 155, doi:10.1007/JHEP10(2012)155, arXiv:1206.3572.

[45] S. Frixione and B. R. Webber, "Matching NLO QCD computations and parton shower simulations", *JHEP* **06** (2002) 029, doi:10.1088/1126-6708/2002/06/029, arXiv:hep-ph/0204244.

[46] H. Voss, A. Höcker, J. Stelzer, and F. Tegenfeldt, "TMVA: Toolkit for Multivariate Data Analysis with ROOT", in *XIth International Workshop on Advanced Computing and Analysis Techniques in Physics Research (ACAT)*, p. 40. 2007. arXiv:physics/0703039.

[47] CMS Collaboration, "Particle-Flow Event Reconstruction in CMS and Performance for Jets, Taus, and MET", CMS Physics Analysis Summary CMS-PAS-PFT-09-001, 2009.

[48] CMS Collaboration, "Commissioning of the Particle-flow Event Reconstruction with the first LHC collisions recorded in the CMS detector", CMS Physics Analysis Summary CMS-PAS-PFT-10-001, 2010.

[49] M. J. Oreglia, "A study of the reactions $\psi' \to \gamma\gamma\psi$". PhD thesis, Stanford University, 1980. SLAC Report SLAC-R-236, see Appendix D.

[50] M. Cacciari, G. P. Salam, and G. Soyez, "The anti-k_t jet clustering algorithm", *JHEP* **04** (2008) 063, doi:10.1088/1126-6708/2008/04/063, arXiv:0802.1189.

[51] CMS Collaboration, "Determination of jet energy calibration and transverse momentum resolution in CMS", *JINST* **6** (2011) P11002, doi:10.1088/1748-0221/6/11/P11002, arXiv:1107.4277.

[52] CMS Collaboration, "Pileup Jet Identification", CMS Physics Analysis Summary CMS-PAS-JME-13-005, 2013.

[53] J. C. Collins and D. E. Soper, "Angular distribution of dileptons in high-energy hadron collisions", *Phys. Rev. D* **16** (1977) 2219, doi:10.1103/PhysRevD.16.2219.

[54] D. L. Rainwater, R. Szalapski, and D. Zeppenfeld, "Probing color-singlet exchange in $Z + 2$-jet events at the CERN LHC", *Phys. Rev. D* **54** (1996) 6680, doi:10.1103/PhysRevD.54.6680, arXiv:hep-ph/9605444.

[55] ATLAS and CMS Collaborations, LHC Higgs Combination Group, "Procedure for the LHC Higgs boson search combination in Summer 2011", Technical Report ATL-PHYS-PUB 2011-11, CMS NOTE 2011/005, CERN, 2011.

[56] CMS Collaboration, "Combined results of searches for the standard model Higgs boson in pp collisions at $\sqrt{s} = 7$ TeV", *Phys. Lett. B* **710** (2012) 26, doi:10.1016/j.physletb.2012.02.064, arXiv:1202.1488.

[57] P. D. Dauncey, M. Kenzie, N. Wardle, and G. J. Davies, "Handling uncertainties in background shapes: the discrete profiling method", *JINST* **10** (2015) P04015, doi:10.1088/1748-0221/10/04/P04015, arXiv:1408.6865.

[58] E. W. Weisstein, "F-Distribution". http://mathworld.wolfram.com/F-Distribution.html, 2014. From MathWorld – A Wolfram Web Resource.

[59] CMS Collaboration, "CMS Luminosity Based on Pixel Cluster Counting - Summer 2013 Update", CMS Physics Analysis Summary CMS-PAS-LUM-13-001, 2013.

[60] CMS Collaboration, "Measurement of the Inclusive W and Z Production Cross Sections in pp Collisions at $\sqrt{s} = 7$ TeV", *JHEP* **10** (2011) 132, doi:10.1007/JHEP10(2011)132, arXiv:1107.4789.

[61] J. Alwall et al., "The automated computation of tree-level and next-to-leading order differential cross sections, and their matching to parton shower simulations", *JHEP* **07** (2014) 079, doi:10.1007/JHEP07(2014)079, arXiv:1405.0301.

[62] A. D. Martin, W. J. Stirling, R. S. Thorne, and G. Watt, "Parton distributions for the LHC", *Eur. Phys. J. C* **63** (2009) 189, doi:10.1140/epjc/s10052-009-1072-5, arXiv:0901.0002.

[63] M. R. Whalley, D. Bourilkov, and R. C. Group, "The Les Houches accord PDFs (LHAPDF) and LHAGLUE", (2005). arXiv:hep-ph/0508110.

[64] P. Artoisenet et al., "A framework for Higgs characterisation", *JHEP* **11** (2013) 043, doi:10.1007/JHEP11(2013)043, arXiv:1306.6464.

[65] R. Frederix and S. Frixione, "Merging meets matching in MC@NLO", *JHEP* **12** (2012) 061, doi:10.1007/JHEP12(2012)061, arXiv:1209.6215.

[66] T. Sjöstrand, S. Mrenna, and P. Skands, "A brief introduction to PYTHIA 8.1", *Comp. Phys. Comm.* **178** (2008) 852, doi:10.1016/j.cpc.2008.01.036, arXiv:0710.3820.

[67] R. Corke and T. Sjöstrand, "Interleaved Parton Showers and Tuning Prospects", *JHEP* **03** (2011) 032, doi:10.1007/JHEP03(2011)032, arXiv:1011.1759.

[68] S. Bolognesi et al., "Spin and parity of a single-produced resonance at the LHC", *Phys. Rev. D* **86** (2012) 095031, doi:10.1103/PhysRevD.86.095031, arXiv:1208.4018.

[69] T. Corbett, O. J. P. Eboli, J. Gonzalez-Fraile, and M. C. Gonzalez-Garcia, "Determining Triple Gauge Boson Couplings from Higgs Data", *Phys. Rev. Lett.* **111** (2013) 011801, doi:10.1103/PhysRevLett.111.011801, arXiv:1304.1151.

[70] C. Degrande et al., "UFO – The Universal FEYNRULES Output", *Comput. Phys. Commun.* **183** (2012) 1201, doi:10.1016/j.cpc.2012.01.022, arXiv:1108.2040.

[71] G. Altarelli, T. Sjöstrand, and F. Zwirner, "Physics at LEP2: Vol. 1", CERN Report CERN-96-01-V-1, 1996. doi:10.5170/CERN-1996-001-V-1.

[72] CMS Collaboration, "Measurement of the W^+W^- cross section in pp Collisions at $\sqrt{s} = 7$ TeV and limits on anomalous $WW\gamma$ and WWZ couplings", *Eur. Phys. J. C* **73** (2013) 2610, doi:10.1140/epjc/s10052-013-2610-8, arXiv:1306.1126.

[73] ATLAS Collaboration, "Measurement of WZ production in proton-proton collisions at $\sqrt{s} = 7$ TeV with the ATLAS detector", *Eur. Phys. J. C* **72** (2012) 2173, doi:10.1140/epjc/s10052-012-2173-0, arXiv:1208.1390.

[74] ATLAS Collaboration, "Measurement of W^+W^- production in pp collisions at $\sqrt{s} = 7$ TeV with the ATLAS detector and limits on anomalous WWZ and $WW\gamma$ couplings", *Phys. Rev. D* **87** (2013) 112001, doi:10.1103/PhysRevD.87.112001, arXiv:1210.2979. [Erratum: doi:10.1103/PhysRevD.88.079906].

[75] CMS Collaboration, "Measurement of the W^+W^- cross section in pp collisions at $\sqrt{s} = 8$ TeV and limits on anomalous gauge couplings", (2015). arXiv:1507.03268.

A Appendix

Table 1: Values of the pp $\rightarrow$ H $\rightarrow$ $\gamma\gamma$ differential cross sections as a function of kinematic observables as measured in data and as predicted in SM simulations. For each observable the fit to $m_{\gamma\gamma}$ is performed simultaneously in all the bins. Since the signal mass is profiled for each observable, the best fit $\hat{m}_{\mathrm{H}}$ varies from observable to observable.

	σ_{obs}[fb]	$(\hat{m}_{\mathrm{H}} = 124.4\,\mathrm{GeV})$	$\sigma_{\mathrm{MADGRAPH5_aMC@NLO+XH}}$	$\sigma_{\mathrm{HRES+XH}}$	$\sigma_{\mathrm{POWHEG+XH}}$
Fiducial cross section		$32.2^{+10.1}_{-9.7}$	$30.3^{+5.9}_{-4.7}$	$31.5^{+4.0}_{-3.0}$	$32.0^{+5.8}_{-4.6}$
$p_{\mathrm{T}}^{\gamma\gamma}$	σ_{obs}[fb]	$(\hat{m}_{\mathrm{H}} = 124.8\,\mathrm{GeV})$	$\sigma_{\mathrm{MADGRAPH5_aMC@NLO+XH}}$	$\sigma_{\mathrm{HRES+XH}}$	$\sigma_{\mathrm{POWHEG+XH}}$
0–15 GeV		$9.0^{+6.4}_{-6.2}$	$7.5^{+1.5}_{-1.2}$	$8.6^{+0.9}_{-0.9}$	$8.6^{+1.6}_{-1.3}$
15–26 GeV		$2.0^{+4.9}_{-5.5}$	$5.9^{+1.2}_{-1.0}$	$6.8^{+0.8}_{-0.7}$	$6.6^{+1.3}_{-1.0}$
26–43 GeV		$3.4^{+4.8}_{-4.6}$	$6.1^{+1.3}_{-1.0}$	$6.3^{+1.0}_{-0.7}$	$6.2^{+1.1}_{-0.9}$
43–72 GeV		$6.2^{+3.7}_{-3.5}$	$5.2^{+1.1}_{-0.9}$	$5.2^{+0.9}_{-0.6}$	$5.1^{+0.9}_{-0.7}$
72–125 GeV		$4.6^{+2.4}_{-2.7}$	$3.4^{+0.7}_{-0.6}$	$3.3^{+0.6}_{-0.4}$	$3.3^{+0.6}_{-0.4}$
125–200 GeV		$2.6^{+1.0}_{-1.0}$	$1.4^{+0.3}_{-0.2}$	$1.3^{+0.3}_{-0.3}$	$1.3^{+0.2}_{-0.2}$
>200 GeV		$0.7^{+0.5}_{-0.4}$	$0.6^{+0.1}_{-0.1}$	$0.5^{+0.1}_{-0.1}$	$0.6^{+0.2}_{-0.1}$
$\lvert\cos\theta^*\rvert$	σ_{obs}[fb]	$(\hat{m}_{\mathrm{H}} = 124.7\,\mathrm{GeV})$	$\sigma_{\mathrm{MADGRAPH5_aMC@NLO+XH}}$	$\sigma_{\mathrm{HRES+XH}}$	$\sigma_{\mathrm{POWHEG+XH}}$
0.00–0.11		$4.9^{+3.3}_{-3.3}$	$4.3^{+0.8}_{-0.7}$	$4.8^{+0.5}_{-0.5}$	$4.6^{+0.8}_{-0.7}$
0.11–0.23		$3.3^{+3.2}_{-3.1}$	$4.7^{+0.9}_{-0.7}$	$5.2^{+0.7}_{-0.6}$	$5.0^{+0.9}_{-0.7}$
0.23–0.36		$11.7^{+3.8}_{-3.5}$	$4.9^{+1.0}_{-0.8}$	$5.4^{+0.7}_{-0.5}$	$5.2^{+0.9}_{-0.7}$
0.36–0.53		$2.4^{+5.6}_{-5.1}$	$6.1^{+1.2}_{-1.0}$	$6.7^{+0.9}_{-0.6}$	$6.4^{+1.2}_{-0.9}$
0.53–1.00		$7.3^{+7.3}_{-7.1}$	$10.2^{+2.0}_{-1.6}$	$9.6^{+1.4}_{-1.0}$	$10.7^{+2.0}_{-1.5}$
$\Delta\phi^{\gamma\gamma}$	σ_{obs}[fb]	$(\hat{m}_{\mathrm{H}} = 124.6\,\mathrm{GeV})$	$\sigma_{\mathrm{MADGRAPH5_aMC@NLO+XH}}$	$\sigma_{\mathrm{HRES+XH}}$	$\sigma_{\mathrm{POWHEG+XH}}$
0.00–0.92		$0.9^{+0.9}_{-0.8}$	$1.1^{+0.2}_{-0.2}$	$0.9^{+0.1}_{-0.1}$	$1.0^{+0.2}_{-0.1}$
0.92–1.72		$2.6^{+1.4}_{-1.6}$	$2.2^{+0.4}_{-0.3}$	$2.0^{+0.3}_{-0.2}$	$2.1^{+0.4}_{-0.3}$
1.72–2.37		$2.2^{+2.6}_{-2.5}$	$4.2^{+0.9}_{-0.7}$	$4.0^{+0.7}_{-0.5}$	$4.2^{+0.7}_{-0.5}$
2.37–2.74		$8.2^{+4.1}_{-3.9}$	$5.9^{+1.2}_{-1.0}$	$5.9^{+0.9}_{-0.7}$	$5.9^{+1.1}_{-0.8}$
2.74–2.97		$2.8^{+4.4}_{-5.4}$	$7.4^{+1.5}_{-1.2}$	$8.2^{+1.1}_{-0.7}$	$8.2^{+1.5}_{-1.2}$
2.97–3.15		$14.4^{+9.0}_{-6.6}$	$9.4^{+1.9}_{-1.5}$	$10.5^{+1.0}_{-1.3}$	$10.6^{+2.0}_{-1.6}$
$\lvert\lvert y^{\gamma\gamma}\rvert\rvert$	σ_{obs}[fb]	$(\hat{m}_{\mathrm{H}} = 124.2\,\mathrm{GeV})$	$\sigma_{\mathrm{MADGRAPH5_aMC@NLO+XH}}$	$\sigma_{\mathrm{HRES+XH}}$	$\sigma_{\mathrm{POWHEG+XH}}$
0.00–0.16		$2.4^{+2.6}_{-2.6}$	$3.1^{+0.6}_{-0.5}$	$3.2^{+0.4}_{-0.3}$	$3.2^{+0.6}_{-0.5}$
0.16–0.35		$2.2^{+2.7}_{-2.6}$	$3.7^{+0.7}_{-0.6}$	$3.7^{+0.5}_{-0.4}$	$3.9^{+0.7}_{-0.6}$
0.35–0.58		$9.5^{+3.3}_{-3.2}$	$4.3^{+0.8}_{-0.7}$	$4.4^{+0.6}_{-0.5}$	$4.5^{+0.8}_{-0.7}$
0.58–0.90		$5.4^{+4.5}_{-3.7}$	$5.6^{+1.1}_{-0.9}$	$5.9^{+0.9}_{-0.6}$	$5.8^{+1.1}_{-0.8}$
0.90–2.50		$15.9^{+11.9}_{-11.1}$	$13.8^{+2.7}_{-2.1}$	$14.4^{+1.8}_{-1.3}$	$14.7^{+2.7}_{-2.1}$
N_{jets}	σ_{obs}[fb]	$(\hat{m}_{\mathrm{H}} = 124.6\,\mathrm{GeV})$	$\sigma_{\mathrm{MADGRAPH5_aMC@NLO+XH}}$	$\sigma_{\mathrm{POWHEG\ HJ+XH}}$	$\sigma_{\mathrm{POWHEG+XH}}$
0		$20.2^{+9.3}_{-9.0}$	$17.4^{+3.5}_{-2.8}$	$18.1^{+6.0}_{-2.5}$	$19.0^{+3.6}_{-2.8}$
1		$4.3^{+6.4}_{-6.3}$	$8.7^{+1.8}_{-1.5}$	$9.6^{+2.2}_{-1.3}$	$9.2^{+1.7}_{-1.3}$
2		$3.9^{+3.7}_{-3.8}$	$3.1^{+0.6}_{-0.5}$	$3.1^{+0.7}_{-0.4}$	$2.8^{+0.5}_{-0.2}$
$\geq$3		$2.5^{+2.2}_{-2.2}$	$1.1^{+0.2}_{-0.2}$	$1.0^{+0.3}_{-0.1}$	$1.0^{+0.2}_{-0.1}$
$p_{\mathrm{T}}^{\mathrm{j1}}$	σ_{obs}[fb]	$(\hat{m}_{\mathrm{H}} = 124.3\,\mathrm{GeV})$	$\sigma_{\mathrm{MADGRAPH5_aMC@NLO+XH}}$	$\sigma_{\mathrm{POWHEG\ HJ+XH}}$	$\sigma_{\mathrm{POWHEG+XH}}$
25–40 GeV		$2.1^{+6.8}_{-6.6}$	$4.4^{+1.0}_{-0.8}$	$4.5^{+1.2}_{-0.6}$	$4.5^{+0.8}_{-0.6}$
40–64 GeV		$6.4^{+5.6}_{-5.0}$	$3.7^{+0.8}_{-0.7}$	$3.9^{+0.9}_{-0.5}$	$3.8^{+0.6}_{-0.5}$
64–104 GeV		$3.4^{+3.4}_{-3.3}$	$2.7^{+0.5}_{-0.4}$	$2.9^{+0.6}_{-0.4}$	$2.7^{+0.4}_{-0.3}$
104–200 GeV		$0.8^{+1.9}_{-1.8}$	$1.6^{+0.3}_{-0.2}$	$1.8^{+0.4}_{-0.3}$	$1.6^{+0.3}_{-0.2}$
>200 GeV		$0.8^{+0.8}_{-0.7}$	$0.4^{+0.1}_{-0.1}$	$0.5^{+0.1}_{-0.1}$	$0.4^{+0.1}_{-0.1}$
$\lvert y^{\gamma\gamma} - y^{\mathrm{j1}}\rvert$	σ_{obs}[fb]	$(\hat{m}_{\mathrm{H}} = 124.5\,\mathrm{GeV})$	$\sigma_{\mathrm{MADGRAPH5_aMC@NLO+XH}}$	$\sigma_{\mathrm{POWHEG\ HJ+XH}}$	$\sigma_{\mathrm{POWHEG+XH}}$
0.00–0.62		$6.1^{+4.0}_{-3.8}$	$3.8^{+0.7}_{-0.6}$	$4.0^{+0.9}_{-0.5}$	$3.7^{+0.6}_{-0.5}$
0.62–1.25		$-1.1^{+4.4}_{-3.6}$	$3.4^{+0.7}_{-0.6}$	$3.6^{+0.8}_{-0.5}$	$3.4^{+0.6}_{-0.5}$
1.25–1.92		$5.2^{+3.0}_{-2.8}$	$2.7^{+0.5}_{-0.5}$	$2.9^{+0.7}_{-0.4}$	$2.7^{+0.5}_{-0.4}$
>1.92		$1.6^{+4.1}_{-4.8}$	$3.0^{+0.6}_{-0.5}$	$3.2^{+0.7}_{-0.5}$	$3.1^{+0.5}_{-0.4}$
m_{jj}	σ_{obs}[fb]	$(\hat{m}_{\mathrm{H}} = 124.7\,\mathrm{GeV})$	$\sigma_{\mathrm{MADGRAPH5_aMC@NLO+XH}}$	$\sigma_{\mathrm{POWHEG\ HJ+XH}}$	$\sigma_{\mathrm{POWHEG+XH}}$
0–153 GeV		$6.8^{+4.5}_{-4.0}$	$3.0^{+0.7}_{-0.6}$	$2.9^{+0.7}_{-0.4}$	$2.6^{+0.4}_{-0.3}$
153–455 GeV		$1.8^{+3.0}_{-3.2}$	$2.1^{+0.4}_{-0.4}$	$2.1^{+0.5}_{-0.3}$	$2.0^{+0.3}_{-0.2}$
455–1000 GeV		$0.3^{+1.2}_{-1.0}$	$0.8^{+0.1}_{-0.1}$	$0.9^{+0.1}_{-0.1}$	$0.8^{+0.1}_{-0.1}$
>1000 GeV		$-0.2^{+0.3}_{-0.2}$	$0.3^{+0.0}_{-0.0}$	$0.3^{+0.0}_{-0.0}$	$0.3^{+0.0}_{-0.0}$
$\Delta\eta^{\mathrm{jj}}$	σ_{obs}[fb]	$(\hat{m}_{\mathrm{H}} = 124.4\,\mathrm{GeV})$	$\sigma_{\mathrm{MADGRAPH5_aMC@NLO+XH}}$	$\sigma_{\mathrm{POWHEG\ HJ+XH}}$	$\sigma_{\mathrm{POWHEG+XH}}$
0.00–1.65		$3.0^{+3.6}_{-3.5}$	$2.9^{+0.6}_{-0.5}$	$2.8^{+0.7}_{-0.4}$	$2.5^{+0.4}_{-0.3}$
1.65–4.30		$3.7^{+2.8}_{-2.6}$	$2.4^{+0.5}_{-0.4}$	$2.3^{+0.5}_{-0.3}$	$2.2^{+0.3}_{-0.3}$
4.30–10.00		$0.1^{+1.0}_{-0.9}$	$0.9^{+0.1}_{-0.1}$	$0.9^{+0.1}_{-0.1}$	$0.9^{+0.1}_{-0.1}$
$\Delta\phi^{\gamma\gamma,\mathrm{jj}}$	σ_{obs}[fb]	$(\hat{m}_{\mathrm{H}} = 124.5\,\mathrm{GeV})$	$\sigma_{\mathrm{MADGRAPH5_aMC@NLO+XH}}$	$\sigma_{\mathrm{POWHEG\ HJ+XH}}$	$\sigma_{\mathrm{POWHEG+XH}}$
0.00–2.95		$-0.1^{+0.2}_{-0.2}$	$0.1^{+0.0}_{-0.0}$	$0.1^{+0.0}_{-0.0}$	$0.1^{+0.0}_{-0.0}$
2.95–3.08		$9.6^{+5.0}_{-4.3}$	$1.9^{+0.4}_{-0.3}$	$1.9^{+0.4}_{-0.3}$	$1.8^{+0.3}_{-0.2}$
3.08–3.15		$-1.1^{+2.5}_{-2.8}$	$1.6^{+0.2}_{-0.2}$	$1.7^{+0.3}_{-0.2}$	$1.6^{+0.2}_{-0.2}$
$\Delta\phi^{\mathrm{jj}}$	σ_{obs}[fb]	$(\hat{m}_{\mathrm{H}} = 124.6\,\mathrm{GeV})$	$\sigma_{\mathrm{MADGRAPH5_aMC@NLO+XH}}$	$\sigma_{\mathrm{POWHEG\ HJ+XH}}$	$\sigma_{\mathrm{POWHEG+XH}}$
0.00–0.88		$1.5^{+2.0}_{-1.9}$	$1.6^{+0.3}_{-0.3}$	$1.7^{+0.3}_{-0.2}$	$1.4^{+0.2}_{-0.2}$
0.88–1.82		$1.1^{+2.1}_{-2.3}$	$1.7^{+0.3}_{-0.3}$	$1.6^{+0.3}_{-0.2}$	$1.6^{+0.3}_{-0.2}$
1.82–3.15		$5.0^{+3.8}_{-3.5}$	$3.0^{+0.6}_{-0.5}$	$2.8^{+0.7}_{-0.4}$	$2.7^{+0.4}_{-0.3}$
$\lvert\eta^{\gamma\gamma} - (\eta^{\mathrm{j1}} + \eta^{\mathrm{j2}})/2\rvert$	σ_{obs}[fb]	$(\hat{m}_{\mathrm{H}} = 124.6\,\mathrm{GeV})$	$\sigma_{\mathrm{MADGRAPH5_aMC@NLO+XH}}$	$\sigma_{\mathrm{POWHEG\ HJ+XH}}$	$\sigma_{\mathrm{POWHEG+XH}}$
0.0–0.5		$1.6^{+1.8}_{-2.1}$	$1.6^{+0.3}_{-0.2}$	$1.6^{+0.3}_{-0.2}$	$1.5^{+0.2}_{-0.2}$
0.5–1.2		$5.8^{+2.4}_{-2.2}$	$1.9^{+0.4}_{-0.3}$	$1.9^{+0.4}_{-0.2}$	$1.7^{+0.3}_{-0.2}$
>1.2		$-0.1^{+3.8}_{-3.7}$	$2.6^{+0.6}_{-0.5}$	$2.6^{+0.6}_{-0.3}$	$2.4^{+0.4}_{-0.3}$

B The CMS Collaboration

Yerevan Physics Institute, Yerevan, Armenia
V. Khachatryan, A.M. Sirunyan, A. Tumasyan

Institut für Hochenergiephysik der OeAW, Wien, Austria
W. Adam, E. Asilar, T. Bergauer, J. Brandstetter, E. Brondolin, M. Dragicevic, J. Erö, M. Flechl, M. Friedl, R. Frühwirth[1], V.M. Ghete, C. Hartl, N. Hörmann, J. Hrubec, M. Jeitler[1], V. Knünz, A. König, M. Krammer[1], I. Krätschmer, D. Liko, T. Matsushita, I. Mikulec, D. Rabady[2], B. Rahbaran, H. Rohringer, J. Schieck[1], R. Schöfbeck, J. Strauss, W. Treberer-Treberspurg, W. Waltenberger, C.-E. Wulz[1]

National Centre for Particle and High Energy Physics, Minsk, Belarus
V. Mossolov, N. Shumeiko, J. Suarez Gonzalez

Universiteit Antwerpen, Antwerpen, Belgium
S. Alderweireldt, T. Cornelis, E.A. De Wolf, X. Janssen, A. Knutsson, J. Lauwers, S. Luyckx, S. Ochesanu, R. Rougny, M. Van De Klundert, H. Van Haevermaet, P. Van Mechelen, N. Van Remortel, A. Van Spilbeeck

Vrije Universiteit Brussel, Brussel, Belgium
S. Abu Zeid, F. Blekman, J. D'Hondt, N. Daci, I. De Bruyn, K. Deroover, N. Heracleous, J. Keaveney, S. Lowette, L. Moreels, A. Olbrechts, Q. Python, D. Strom, S. Tavernier, W. Van Doninck, P. Van Mulders, G.P. Van Onsem, I. Van Parijs

Université Libre de Bruxelles, Bruxelles, Belgium
P. Barria, C. Caillol, B. Clerbaux, G. De Lentdecker, H. Delannoy, D. Dobur, G. Fasanella, L. Favart, A.P.R. Gay, A. Grebenyuk, T. Lenzi, A. Léonard, T. Maerschalk, A. Marinov, L. Perniè, A. Randle-conde, T. Reis, T. Seva, C. Vander Velde, P. Vanlaer, R. Yonamine, F. Zenoni, F. Zhang[3]

Ghent University, Ghent, Belgium
K. Beernaert, L. Benucci, A. Cimmino, S. Crucy, A. Fagot, G. Garcia, M. Gul, J. Mccartin, A.A. Ocampo Rios, D. Poyraz, D. Ryckbosch, S. Salva, M. Sigamani, N. Strobbe, M. Tytgat, W. Van Driessche, E. Yazgan, N. Zaganidis

Université Catholique de Louvain, Louvain-la-Neuve, Belgium
S. Basegmez, C. Beluffi[4], O. Bondu, S. Brochet, G. Bruno, R. Castello, A. Caudron, L. Ceard, G.G. Da Silveira, C. Delaere, D. Favart, L. Forthomme, A. Giammanco[5], J. Hollar, A. Jafari, P. Jez, M. Komm, V. Lemaitre, A. Mertens, C. Nuttens, L. Perrini, A. Pin, K. Piotrzkowski, A. Popov[6], L. Quertenmont, M. Selvaggi, M. Vidal Marono

Université de Mons, Mons, Belgium
N. Beliy, G.H. Hammad

Centro Brasileiro de Pesquisas Fisicas, Rio de Janeiro, Brazil
W.L. Aldá Júnior, G.A. Alves, L. Brito, M. Correa Martins Junior, T. Dos Reis Martins, C. Hensel, C. Mora Herrera, A. Moraes, M.E. Pol, P. Rebello Teles

Universidade do Estado do Rio de Janeiro, Rio de Janeiro, Brazil
E. Belchior Batista Das Chagas, W. Carvalho, J. Chinellato[7], A. Custódio, E.M. Da Costa, D. De Jesus Damiao, C. De Oliveira Martins, S. Fonseca De Souza, L.M. Huertas Guativa, H. Malbouisson, D. Matos Figueiredo, L. Mundim, H. Nogima, W.L. Prado Da Silva, A. Santoro, A. Sznajder, E.J. Tonelli Manganote[7], A. Vilela Pereira

Universidade Estadual Paulista [a], Universidade Federal do ABC [b], São Paulo, Brazil
S. Ahuja[a], C.A. Bernardes[b], A. De Souza Santos[b], S. Dogra[a], T.R. Fernandez Perez Tomei[a], E.M. Gregores[b], P.G. Mercadante[b], C.S. Moon[a,8], S.F. Novaes[a], Sandra S. Padula[a], D. Romero Abad, J.C. Ruiz Vargas

Institute for Nuclear Research and Nuclear Energy, Sofia, Bulgaria
A. Aleksandrov, V. Genchev[†], R. Hadjiiska, P. Iaydjiev, S. Piperov, M. Rodozov, S. Stoykova, G. Sultanov, M. Vutova

University of Sofia, Sofia, Bulgaria
A. Dimitrov, I. Glushkov, L. Litov, B. Pavlov, P. Petkov

Institute of High Energy Physics, Beijing, China
M. Ahmad, J.G. Bian, G.M. Chen, H.S. Chen, M. Chen, T. Cheng, R. Du, C.H. Jiang, R. Plestina[9], F. Romeo, S.M. Shaheen, J. Tao, C. Wang, Z. Wang, H. Zhang

State Key Laboratory of Nuclear Physics and Technology, Peking University, Beijing, China
C. Asawatangtrakuldee, Y. Ban, Q. Li, S. Liu, Y. Mao, S.J. Qian, D. Wang, Z. Xu, W. Zou

Universidad de Los Andes, Bogota, Colombia
C. Avila, A. Cabrera, L.F. Chaparro Sierra, C. Florez, J.P. Gomez, B. Gomez Moreno, J.C. Sanabria

University of Split, Faculty of Electrical Engineering, Mechanical Engineering and Naval Architecture, Split, Croatia
N. Godinovic, D. Lelas, D. Polic, I. Puljak, P.M. Ribeiro Cipriano

University of Split, Faculty of Science, Split, Croatia
Z. Antunovic, M. Kovac

Institute Rudjer Boskovic, Zagreb, Croatia
V. Brigljevic, K. Kadija, J. Luetic, S. Micanovic, L. Sudic

University of Cyprus, Nicosia, Cyprus
A. Attikis, G. Mavromanolakis, J. Mousa, C. Nicolaou, F. Ptochos, P.A. Razis, H. Rykaczewski

Charles University, Prague, Czech Republic
M. Bodlak, M. Finger[10], M. Finger Jr.[10]

Academy of Scientific Research and Technology of the Arab Republic of Egypt, Egyptian Network of High Energy Physics, Cairo, Egypt
A.A. Abdelalim[11], A. Awad[12,13], A. Mahrous[14], A. Radi[13,12]

National Institute of Chemical Physics and Biophysics, Tallinn, Estonia
B. Calpas, M. Kadastik, M. Murumaa, M. Raidal, A. Tiko, C. Veelken

Department of Physics, University of Helsinki, Helsinki, Finland
P. Eerola, J. Pekkanen, M. Voutilainen

Helsinki Institute of Physics, Helsinki, Finland
J. Härkönen, V. Karimäki, R. Kinnunen, T. Lampén, K. Lassila-Perini, S. Lehti, T. Lindén, P. Luukka, T. Mäenpää, T. Peltola, E. Tuominen, J. Tuominiemi, E. Tuovinen, L. Wendland

Lappeenranta University of Technology, Lappeenranta, Finland
J. Talvitie, T. Tuuva

DSM/IRFU, CEA/Saclay, Gif-sur-Yvette, France
M. Besancon, F. Couderc, M. Dejardin, D. Denegri, B. Fabbro, J.L. Faure, C. Favaro, F. Ferri, S. Ganjour, A. Givernaud, P. Gras, G. Hamel de Monchenault, P. Jarry, E. Locci, M. Machet, J. Malcles, J. Rander, A. Rosowsky, M. Titov, A. Zghiche

Laboratoire Leprince-Ringuet, Ecole Polytechnique, IN2P3-CNRS, Palaiseau, France
I. Antropov, S. Baffioni, F. Beaudette, P. Busson, L. Cadamuro, E. Chapon, C. Charlot, T. Dahms, O. Davignon, N. Filipovic, A. Florent, R. Granier de Cassagnac, S. Lisniak, L. Mastrolorenzo, P. Miné, I.N. Naranjo, M. Nguyen, C. Ochando, G. Ortona, P. Paganini, S. Regnard, R. Salerno, J.B. Sauvan, Y. Sirois, T. Strebler, Y. Yilmaz, A. Zabi

Institut Pluridisciplinaire Hubert Curien, Université de Strasbourg, Université de Haute Alsace Mulhouse, CNRS/IN2P3, Strasbourg, France
J.-L. Agram[15], J. Andrea, A. Aubin, D. Bloch, J.-M. Brom, M. Buttignol, E.C. Chabert, N. Chanon, C. Collard, E. Conte[15], X. Coubez, J.-C. Fontaine[15], D. Gelé, U. Goerlach, C. Goetzmann, A.-C. Le Bihan, J.A. Merlin[2], K. Skovpen, P. Van Hove

Centre de Calcul de l'Institut National de Physique Nucleaire et de Physique des Particules, CNRS/IN2P3, Villeurbanne, France
S. Gadrat

Université de Lyon, Université Claude Bernard Lyon 1, CNRS-IN2P3, Institut de Physique Nucléaire de Lyon, Villeurbanne, France
S. Beauceron, C. Bernet, G. Boudoul, E. Bouvier, C.A. Carrillo Montoya, J. Chasserat, R. Chierici, D. Contardo, B. Courbon, P. Depasse, H. El Mamouni, J. Fan, J. Fay, S. Gascon, M. Gouzevitch, B. Ille, F. Lagarde, I.B. Laktineh, M. Lethuillier, L. Mirabito, A.L. Pequegnot, S. Perries, J.D. Ruiz Alvarez, D. Sabes, L. Sgandurra, V. Sordini, M. Vander Donckt, P. Verdier, S. Viret, H. Xiao

Georgian Technical University, Tbilisi, Georgia
T. Toriashvili[16]

Tbilisi State University, Tbilisi, Georgia
Z. Tsamalaidze[10]

RWTH Aachen University, I. Physikalisches Institut, Aachen, Germany
C. Autermann, S. Beranek, M. Edelhoff, L. Feld, A. Heister, M.K. Kiesel, K. Klein, M. Lipinski, A. Ostapchuk, M. Preuten, F. Raupach, S. Schael, J.F. Schulte, T. Verlage, H. Weber, B. Wittmer, V. Zhukov[6]

RWTH Aachen University, III. Physikalisches Institut A, Aachen, Germany
M. Ata, M. Brodski, E. Dietz-Laursonn, D. Duchardt, M. Endres, M. Erdmann, S. Erdweg, T. Esch, R. Fischer, A. Güth, T. Hebbeker, C. Heidemann, K. Hoepfner, D. Klingebiel, S. Knutzen, P. Kreuzer, M. Merschmeyer, A. Meyer, P. Millet, M. Olschewski, K. Padeken, P. Papacz, T. Pook, M. Radziej, H. Reithler, M. Rieger, F. Scheuch, L. Sonnenschein, D. Teyssier, S. Thüer

RWTH Aachen University, III. Physikalisches Institut B, Aachen, Germany
V. Cherepanov, Y. Erdogan, G. Flügge, H. Geenen, M. Geisler, F. Hoehle, B. Kargoll, T. Kress, Y. Kuessel, A. Künsken, J. Lingemann[2], A. Nehrkorn, A. Nowack, I.M. Nugent, C. Pistone, O. Pooth, A. Stahl

Deutsches Elektronen-Synchrotron, Hamburg, Germany
M. Aldaya Martin, I. Asin, N. Bartosik, O. Behnke, U. Behrens, A.J. Bell, K. Borras, A. Burgmeier, A. Cakir, L. Calligaris, A. Campbell, S. Choudhury, F. Costanza, C. Diez

Pardos, G. Dolinska, S. Dooling, T. Dorland, G. Eckerlin, D. Eckstein, T. Eichhorn, G. Flucke, E. Gallo, J. Garay Garcia, A. Geiser, A. Gizhko, P. Gunnellini, J. Hauk, M. Hempel[17], H. Jung, A. Kalogeropoulos, O. Karacheban[17], M. Kasemann, P. Katsas, J. Kieseler, C. Kleinwort, I. Korol, W. Lange, J. Leonard, K. Lipka, A. Lobanov, W. Lohmann[17], R. Mankel, I. Marfin[17], I.-A. Melzer-Pellmann, A.B. Meyer, G. Mittag, J. Mnich, A. Mussgiller, S. Naumann-Emme, A. Nayak, E. Ntomari, H. Perrey, D. Pitzl, R. Placakyte, A. Raspereza, B. Roland, M.Ö. Sahin, P. Saxena, T. Schoerner-Sadenius, M. Schröder, C. Seitz, S. Spannagel, K.D. Trippkewitz, R. Walsh, C. Wissing

University of Hamburg, Hamburg, Germany
V. Blobel, M. Centis Vignali, A.R. Draeger, J. Erfle, E. Garutti, K. Goebel, D. Gonzalez, M. Görner, J. Haller, M. Hoffmann, R.S. Höing, A. Junkes, R. Klanner, R. Kogler, T. Lapsien, T. Lenz, I. Marchesini, D. Marconi, D. Nowatschin, J. Ott, F. Pantaleo[2], T. Peiffer, A. Perieanu, N. Pietsch, J. Poehlsen, D. Rathjens, C. Sander, H. Schettler, P. Schleper, E. Schlieckau, A. Schmidt, J. Schwandt, M. Seidel, V. Sola, H. Stadie, G. Steinbrück, H. Tholen, D. Troendle, E. Usai, L. Vanelderen, A. Vanhoefer

Institut für Experimentelle Kernphysik, Karlsruhe, Germany
M. Akbiyik, C. Barth, C. Baus, J. Berger, C. Böser, E. Butz, T. Chwalek, F. Colombo, W. De Boer, A. Descroix, A. Dierlamm, S. Fink, F. Frensch, M. Giffels, A. Gilbert, F. Hartmann[2], S.M. Heindl, U. Husemann, F. Kassel[2], I. Katkov[6], A. Kornmayer[2], P. Lobelle Pardo, B. Maier, H. Mildner, M.U. Mozer, T. Müller, Th. Müller, M. Plagge, G. Quast, K. Rabbertz, S. Röcker, F. Roscher, H.J. Simonis, F.M. Stober, R. Ulrich, J. Wagner-Kuhr, S. Wayand, M. Weber, T. Weiler, C. Wöhrmann, R. Wolf

Institute of Nuclear and Particle Physics (INPP), NCSR Demokritos, Aghia Paraskevi, Greece
G. Anagnostou, G. Daskalakis, T. Geralis, V.A. Giakoumopoulou, A. Kyriakis, D. Loukas, A. Psallidas, I. Topsis-Giotis

University of Athens, Athens, Greece
A. Agapitos, S. Kesisoglou, A. Panagiotou, N. Saoulidou, E. Tziaferi

University of Ioánnina, Ioánnina, Greece
I. Evangelou, G. Flouris, C. Foudas, P. Kokkas, N. Loukas, N. Manthos, I. Papadopoulos, E. Paradas, J. Strologas

Wigner Research Centre for Physics, Budapest, Hungary
G. Bencze, C. Hajdu, A. Hazi, P. Hidas, D. Horvath[18], F. Sikler, V. Veszpremi, G. Vesztergombi[19], A.J. Zsigmond

Institute of Nuclear Research ATOMKI, Debrecen, Hungary
N. Beni, S. Czellar, J. Karancsi[20], J. Molnar, Z. Szillasi

University of Debrecen, Debrecen, Hungary
M. Bartók[21], A. Makovec, P. Raics, Z.L. Trocsanyi, B. Ujvari

National Institute of Science Education and Research, Bhubaneswar, India
P. Mal, K. Mandal, N. Sahoo, S.K. Swain

Panjab University, Chandigarh, India
S. Bansal, S.B. Beri, V. Bhatnagar, R. Chawla, R. Gupta, U.Bhawandeep, A.K. Kalsi, A. Kaur, M. Kaur, R. Kumar, A. Mehta, M. Mittal, N. Nishu, J.B. Singh, G. Walia

University of Delhi, Delhi, India
Ashok Kumar, Arun Kumar, A. Bhardwaj, B.C. Choudhary, R.B. Garg, A. Kumar, S. Malhotra, M. Naimuddin, K. Ranjan, R. Sharma, V. Sharma

Saha Institute of Nuclear Physics, Kolkata, India
S. Banerjee, S. Bhattacharya, K. Chatterjee, S. Dey, S. Dutta, Sa. Jain, R. Khurana, N. Majumdar, A. Modak, K. Mondal, S. Mukherjee, S. Mukhopadhyay, A. Roy, D. Roy, S. Roy Chowdhury, S. Sarkar, M. Sharan

Bhabha Atomic Research Centre, Mumbai, India
A. Abdulsalam, R. Chudasama, D. Dutta, V. Jha, V. Kumar, A.K. Mohanty[2], L.M. Pant, P. Shukla, A. Topkar

Tata Institute of Fundamental Research, Mumbai, India
T. Aziz, S. Banerjee, S. Bhowmik[22], R.M. Chatterjee, R.K. Dewanjee, S. Dugad, S. Ganguly, S. Ghosh, M. Guchait, A. Gurtu[23], G. Kole, S. Kumar, B. Mahakud, M. Maity[22], G. Majumder, K. Mazumdar, S. Mitra, G.B. Mohanty, B. Parida, T. Sarkar[22], K. Sudhakar, N. Sur, B. Sutar, N. Wickramage[24]

Indian Institute of Science Education and Research (IISER), Pune, India
S. Sharma

Institute for Research in Fundamental Sciences (IPM), Tehran, Iran
H. Bakhshiansohi, H. Behnamian, S.M. Etesami[25], A. Fahim[26], R. Goldouzian, M. Khakzad, M. Mohammadi Najafabadi, M. Naseri, S. Paktinat Mehdiabadi, F. Rezaei Hosseinabadi, B. Safarzadeh[27], M. Zeinali

University College Dublin, Dublin, Ireland
M. Felcini, M. Grunewald

INFN Sezione di Bari [a], Università di Bari [b], Politecnico di Bari [c], Bari, Italy
M. Abbrescia[a,b], C. Calabria[a,b], C. Caputo[a,b], S.S. Chhibra[a,b], A. Colaleo[a], D. Creanza[a,c], L. Cristella[a,b], N. De Filippis[a,c], M. De Palma[a,b], L. Fiore[a], G. Iaselli[a,c], G. Maggi[a,c], M. Maggi[a], G. Miniello[a,b], S. My[a,c], S. Nuzzo[a,b], A. Pompili[a,b], G. Pugliese[a,c], R. Radogna[a,b], A. Ranieri[a], G. Selvaggi[a,b], L. Silvestris[a,2], R. Venditti[a,b], P. Verwilligen[a]

INFN Sezione di Bologna [a], Università di Bologna [b], Bologna, Italy
G. Abbiendi[a], C. Battilana[2], A.C. Benvenuti[a], D. Bonacorsi[a,b], S. Braibant-Giacomelli[a,b], L. Brigliadori[a,b], R. Campanini[a,b], P. Capiluppi[a,b], A. Castro[a,b], F.R. Cavallo[a], G. Codispoti[a,b], M. Cuffiani[a,b], G.M. Dallavalle[a], F. Fabbri[a], A. Fanfani[a,b], D. Fasanella[a,b], P. Giacomelli[a], C. Grandi[a], L. Guiducci[a,b], S. Marcellini[a], G. Masetti[a], A. Montanari[a], F.L. Navarria[a,b], A. Perrotta[a], A.M. Rossi[a,b], T. Rovelli[a,b], G.P. Siroli[a,b], N. Tosi[a,b], R. Travaglini[a,b]

INFN Sezione di Catania [a], Università di Catania [b], CSFNSM [c], Catania, Italy
G. Cappello[a], M. Chiorboli[a,b], S. Costa[a,b], F. Giordano[a], R. Potenza[a,b], A. Tricomi[a,b], C. Tuve[a,b]

INFN Sezione di Firenze [a], Università di Firenze [b], Firenze, Italy
G. Barbagli[a], V. Ciulli[a,b], C. Civinini[a], R. D'Alessandro[a,b], E. Focardi[a,b], S. Gonzi[a,b], V. Gori[a,b], P. Lenzi[a,b], M. Meschini[a], S. Paoletti[a], G. Sguazzoni[a], A. Tropiano[a,b], L. Viliani[a,b]

INFN Laboratori Nazionali di Frascati, Frascati, Italy
L. Benussi, S. Bianco, F. Fabbri, D. Piccolo

INFN Sezione di Genova [a], Università di Genova [b], Genova, Italy
V. Calvelli[a,b], F. Ferro[a], M. Lo Vetere[a,b], M.R. Monge[a,b], E. Robutti[a], S. Tosi[a,b]

INFN Sezione di Milano-Bicocca [a], Università di Milano-Bicocca [b], Milano, Italy
L. Brianza, M.E. Dinardo[a,b], S. Fiorendi[a,b], S. Gennai[a], R. Gerosa[a,b], A. Ghezzi[a,b], P. Govoni[a,b], S. Malvezzi[a], R.A. Manzoni[a,b], B. Marzocchi[a,b,2], D. Menasce[a], L. Moroni[a], M. Paganoni[a,b], D. Pedrini[a], S. Ragazzi[a,b], N. Redaelli[a], T. Tabarelli de Fatis[a,b]

INFN Sezione di Napoli [a], Università di Napoli 'Federico II' [b], Napoli, Italy, Università della Basilicata [c], Potenza, Italy, Università G. Marconi [d], Roma, Italy
S. Buontempo[a], N. Cavallo[a,c], S. Di Guida[a,d,2], M. Esposito[a,b], F. Fabozzi[a,c], A.O.M. Iorio[a,b], G. Lanza[a], L. Lista[a], S. Meola[a,d,2], M. Merola[a], P. Paolucci[a,2], C. Sciacca[a,b], F. Thyssen

INFN Sezione di Padova [a], Università di Padova [b], Padova, Italy, Università di Trento [c], Trento, Italy
P. Azzi[a,2], N. Bacchetta[a], D. Bisello[a,b], A. Boletti[a,b], R. Carlin[a,b], P. Checchia[a], M. Dall'Osso[a,b,2], T. Dorigo[a], U. Dosselli[a], S. Fantinel[a], F. Fanzago[a], F. Gasparini[a,b], U. Gasparini[a,b], F. Gonella[a], A. Gozzelino[a], S. Lacaprara[a], M. Margoni[a,b], A.T. Meneguzzo[a,b], J. Pazzini[a,b], N. Pozzobon[a,b], P. Ronchese[a,b], F. Simonetto[a,b], E. Torassa[a], M. Tosi[a,b], M. Zanetti, P. Zotto[a,b], A. Zucchetta[a,b,2], G. Zumerle[a,b]

INFN Sezione di Pavia [a], Università di Pavia [b], Pavia, Italy
A. Braghieri[a], A. Magnani[a], P. Montagna[a,b], S.P. Ratti[a,b], V. Re[a], C. Riccardi[a,b], P. Salvini[a], I. Vai[a], P. Vitulo[a,b]

INFN Sezione di Perugia [a], Università di Perugia [b], Perugia, Italy
L. Alunni Solestizi[a,b], M. Biasini[a,b], G.M. Bilei[a], D. Ciangottini[a,b,2], L. Fanò[a,b], P. Lariccia[a,b], G. Mantovani[a,b], M. Menichelli[a], A. Saha[a], A. Santocchia[a,b], A. Spiezia[a,b]

INFN Sezione di Pisa [a], Università di Pisa [b], Scuola Normale Superiore di Pisa [c], Pisa, Italy
K. Androsov[a,28], P. Azzurri[a], G. Bagliesi[a], J. Bernardini[a], T. Boccali[a], G. Broccolo[a,c], R. Castaldi[a], M.A. Ciocci[a,28], R. Dell'Orso[a], S. Donato[a,c,2], G. Fedi, L. Foà[a,c†], A. Giassi[a], M.T. Grippo[a,28], F. Ligabue[a,c], T. Lomtadze[a], L. Martini[a,b], A. Messineo[a,b], F. Palla[a], A. Rizzi[a,b], A. Savoy-Navarro[a,29], A.T. Serban[a], P. Spagnolo[a], P. Squillacioti[a,28], R. Tenchini[a], G. Tonelli[a,b], A. Venturi[a], P.G. Verdini[a]

INFN Sezione di Roma [a], Università di Roma [b], Roma, Italy
L. Barone[a,b], F. Cavallari[a], G. D'imperio[a,b,2], D. Del Re[a,b], M. Diemoz[a], S. Gelli[a,b], C. Jorda[a], E. Longo[a,b], F. Margaroli[a,b], P. Meridiani[a], F. Micheli[a,b], G. Organtini[a,b], R. Paramatti[a], F. Preiato[a,b], S. Rahatlou[a,b], C. Rovelli[a], F. Santanastasio[a,b], P. Traczyk[a,b,2]

INFN Sezione di Torino [a], Università di Torino [b], Torino, Italy, Università del Piemonte Orientale [c], Novara, Italy
N. Amapane[a,b], R. Arcidiacono[a,c,2], S. Argiro[a,b], M. Arneodo[a,c], R. Bellan[a,b], C. Biino[a], N. Cartiglia[a], M. Costa[a,b], R. Covarelli[a,b], A. Degano[a,b], N. Demaria[a], L. Finco[a,b,2], B. Kiani[a,b], C. Mariotti[a], S. Maselli[a], E. Migliore[a,b], V. Monaco[a,b], E. Monteil[a,b], M. Musich[a], M.M. Obertino[a,b], L. Pacher[a,b], N. Pastrone[a], M. Pelliccioni[a], G.L. Pinna Angioni[a,b], F. Ravera[a,b], A. Romero[a,b], M. Ruspa[a,c], R. Sacchi[a,b], A. Solano[a,b], A. Staiano[a], U. Tamponi[a]

INFN Sezione di Trieste [a], Università di Trieste [b], Trieste, Italy
S. Belforte[a], V. Candelise[a,b,2], M. Casarsa[a], F. Cossutti[a], G. Della Ricca[a,b], B. Gobbo[a], C. La Licata[a,b], M. Marone[a,b], A. Schizzi[a,b], T. Umer[a,b], A. Zanetti[a]

Kangwon National University, Chunchon, Korea
S. Chang, A. Kropivnitskaya, S.K. Nam

Kyungpook National University, Daegu, Korea
D.H. Kim, G.N. Kim, M.S. Kim, D.J. Kong, S. Lee, Y.D. Oh, A. Sakharov, D.C. Son

Chonbuk National University, Jeonju, Korea
J.A. Brochero Cifuentes, H. Kim, T.J. Kim, M.S. Ryu

Chonnam National University, Institute for Universe and Elementary Particles, Kwangju, Korea
S. Song

Korea University, Seoul, Korea
S. Choi, Y. Go, D. Gyun, B. Hong, M. Jo, H. Kim, Y. Kim, B. Lee, K. Lee, K.S. Lee, S. Lee, S.K. Park, Y. Roh

Seoul National University, Seoul, Korea
H.D. Yoo

University of Seoul, Seoul, Korea
M. Choi, H. Kim, J.H. Kim, J.S.H. Lee, I.C. Park, G. Ryu

Sungkyunkwan University, Suwon, Korea
Y. Choi, Y.K. Choi, J. Goh, D. Kim, E. Kwon, J. Lee, I. Yu

Vilnius University, Vilnius, Lithuania
A. Juodagalvis, J. Vaitkus

National Centre for Particle Physics, Universiti Malaya, Kuala Lumpur, Malaysia
I. Ahmed, Z.A. Ibrahim, J.R. Komaragiri, M.A.B. Md Ali[30], F. Mohamad Idris[31], W.A.T. Wan Abdullah

Centro de Investigacion y de Estudios Avanzados del IPN, Mexico City, Mexico
E. Casimiro Linares, H. Castilla-Valdez, E. De La Cruz-Burelo, I. Heredia-de La Cruz[32], A. Hernandez-Almada, R. Lopez-Fernandez, A. Sanchez-Hernandez

Universidad Iberoamericana, Mexico City, Mexico
S. Carrillo Moreno, F. Vazquez Valencia

Benemerita Universidad Autonoma de Puebla, Puebla, Mexico
S. Carpinteyro, I. Pedraza, H.A. Salazar Ibarguen

Universidad Autónoma de San Luis Potosí, San Luis Potosí, Mexico
A. Morelos Pineda

University of Auckland, Auckland, New Zealand
D. Krofcheck

University of Canterbury, Christchurch, New Zealand
P.H. Butler, S. Reucroft

National Centre for Physics, Quaid-I-Azam University, Islamabad, Pakistan
A. Ahmad, M. Ahmad, Q. Hassan, H.R. Hoorani, W.A. Khan, T. Khurshid, M. Shoaib

National Centre for Nuclear Research, Swierk, Poland
H. Bialkowska, M. Bluj, B. Boimska, T. Frueboes, M. Górski, M. Kazana, K. Nawrocki, K. Romanowska-Rybinska, M. Szleper, P. Zalewski

Institute of Experimental Physics, Faculty of Physics, University of Warsaw, Warsaw, Poland
G. Brona, K. Bunkowski, K. Doroba, A. Kalinowski, M. Konecki, J. Krolikowski, M. Misiura, M. Olszewski, M. Walczak

Laboratório de Instrumentação e Física Experimental de Partículas, Lisboa, Portugal
P. Bargassa, C. Beirão Da Cruz E Silva, A. Di Francesco, P. Faccioli, P.G. Ferreira Parracho, M. Gallinaro, N. Leonardo, L. Lloret Iglesias, F. Nguyen, J. Rodrigues Antunes, J. Seixas, O. Toldaiev, D. Vadruccio, J. Varela, P. Vischia

Joint Institute for Nuclear Research, Dubna, Russia
S. Afanasiev, P. Bunin, M. Gavrilenko, I. Golutvin, I. Gorbunov, A. Kamenev, V. Karjavin, V. Konoplyanikov, A. Lanev, A. Malakhov, V. Matveev[33], P. Moisenz, V. Palichik, V. Perelygin, S. Shmatov, S. Shulha, N. Skatchkov, V. Smirnov, A. Zarubin

Petersburg Nuclear Physics Institute, Gatchina (St. Petersburg), Russia
V. Golovtsov, Y. Ivanov, V. Kim[34], E. Kuznetsova, P. Levchenko, V. Murzin, V. Oreshkin, I. Smirnov, V. Sulimov, L. Uvarov, S. Vavilov, A. Vorobyev

Institute for Nuclear Research, Moscow, Russia
Yu. Andreev, A. Dermenev, S. Gninenko, N. Golubev, A. Karneyeu, M. Kirsanov, N. Krasnikov, A. Pashenkov, D. Tlisov, A. Toropin

Institute for Theoretical and Experimental Physics, Moscow, Russia
V. Epshteyn, V. Gavrilov, N. Lychkovskaya, V. Popov, I. Pozdnyakov, G. Safronov, A. Spiridonov, E. Vlasov, A. Zhokin

National Research Nuclear University 'Moscow Engineering Physics Institute' (MEPhI), Moscow, Russia
A. Bylinkin

P.N. Lebedev Physical Institute, Moscow, Russia
V. Andreev, M. Azarkin[35], I. Dremin[35], M. Kirakosyan, A. Leonidov[35], G. Mesyats, S.V. Rusakov, A. Vinogradov

Skobeltsyn Institute of Nuclear Physics, Lomonosov Moscow State University, Moscow, Russia
A. Baskakov, A. Belyaev, E. Boos, M. Dubinin[36], L. Dudko, A. Ershov, A. Gribushin, V. Klyukhin, O. Kodolova, I. Lokhtin, I. Myagkov, S. Obraztsov, S. Petrushanko, V. Savrin, A. Snigirev

State Research Center of Russian Federation, Institute for High Energy Physics, Protvino, Russia
I. Azhgirey, I. Bayshev, S. Bitioukov, V. Kachanov, A. Kalinin, D. Konstantinov, V. Krychkine, V. Petrov, R. Ryutin, A. Sobol, L. Tourtchanovitch, S. Troshin, N. Tyurin, A. Uzunian, A. Volkov

University of Belgrade, Faculty of Physics and Vinca Institute of Nuclear Sciences, Belgrade, Serbia
P. Adzic[37], M. Ekmedzic, J. Milosevic, V. Rekovic

Centro de Investigaciones Energéticas Medioambientales y Tecnológicas (CIEMAT), Madrid, Spain
J. Alcaraz Maestre, E. Calvo, M. Cerrada, M. Chamizo Llatas, N. Colino, B. De La Cruz, A. Delgado Peris, D. Domínguez Vázquez, A. Escalante Del Valle, C. Fernandez Bedoya, J.P. Fernández Ramos, J. Flix, M.C. Fouz, P. Garcia-Abia, O. Gonzalez Lopez, S. Goy Lopez,

J.M. Hernandez, M.I. Josa, E. Navarro De Martino, A. Pérez-Calero Yzquierdo, J. Puerta Pelayo, A. Quintario Olmeda, I. Redondo, L. Romero, M.S. Soares

Universidad Autónoma de Madrid, Madrid, Spain
C. Albajar, J.F. de Trocóniz, M. Missiroli, D. Moran

Universidad de Oviedo, Oviedo, Spain
H. Brun, J. Cuevas, J. Fernandez Menendez, S. Folgueras, I. Gonzalez Caballero, E. Palencia Cortezon, J.M. Vizan Garcia

Instituto de Física de Cantabria (IFCA), CSIC-Universidad de Cantabria, Santander, Spain
I.J. Cabrillo, A. Calderon, J.R. Castiñeiras De Saa, P. De Castro Manzano, J. Duarte Campderros, M. Fernandez, G. Gomez, A. Graziano, A. Lopez Virto, J. Marco, R. Marco, C. Martinez Rivero, F. Matorras, F.J. Munoz Sanchez, J. Piedra Gomez, T. Rodrigo, A.Y. Rodríguez-Marrero, A. Ruiz-Jimeno, L. Scodellaro, I. Vila, R. Vilar Cortabitarte

CERN, European Organization for Nuclear Research, Geneva, Switzerland
D. Abbaneo, E. Auffray, G. Auzinger, M. Bachtis, P. Baillon, A.H. Ball, D. Barney, A. Benaglia, J. Bendavid, L. Benhabib, J.F. Benitez, G.M. Berruti, P. Bloch, A. Bocci, A. Bonato, C. Botta, H. Breuker, T. Camporesi, G. Cerminara, S. Colafranceschi[38], M. D'Alfonso, D. d'Enterria, A. Dabrowski, V. Daponte, A. David, M. De Gruttola, F. De Guio, A. De Roeck, S. De Visscher, E. Di Marco, M. Dobson, M. Dordevic, T. du Pree, N. Dupont, A. Elliott-Peisert, G. Franzoni, W. Funk, D. Gigi, K. Gill, D. Giordano, M. Girone, F. Glege, R. Guida, S. Gundacker, M. Guthoff, J. Hammer, M. Hansen, P. Harris, J. Hegeman, V. Innocente, P. Janot, H. Kirschenmann, M.J. Kortelainen, K. Kousouris, K. Krajczar, P. Lecoq, C. Lourenço, M.T. Lucchini, N. Magini, L. Malgeri, M. Mannelli, A. Martelli, L. Masetti, F. Meijers, S. Mersi, E. Meschi, F. Moortgat, S. Morovic, M. Mulders, M.V. Nemallapudi, H. Neugebauer, S. Orfanelli[39], L. Orsini, L. Pape, E. Perez, A. Petrilli, G. Petrucciani, A. Pfeiffer, D. Piparo, A. Racz, G. Rolandi[40], M. Rovere, M. Ruan, H. Sakulin, C. Schäfer, C. Schwick, A. Sharma, P. Silva, M. Simon, P. Sphicas[41], D. Spiga, J. Steggemann, B. Stieger, M. Stoye, Y. Takahashi, D. Treille, A. Tsirou, G.I. Veres[19], N. Wardle, H.K. Wöhri, A. Zagozdzinska[42], W.D. Zeuner

Paul Scherrer Institut, Villigen, Switzerland
W. Bertl, K. Deiters, W. Erdmann, R. Horisberger, Q. Ingram, H.C. Kaestli, D. Kotlinski, U. Langenegger, D. Renker, T. Rohe

Institute for Particle Physics, ETH Zurich, Zurich, Switzerland
F. Bachmair, L. Bäni, L. Bianchini, M.A. Buchmann, B. Casal, G. Dissertori, M. Dittmar, M. Donegà, M. Dünser, P. Eller, C. Grab, C. Heidegger, D. Hits, J. Hoss, G. Kasieczka, W. Lustermann, B. Mangano, A.C. Marini, M. Marionneau, P. Martinez Ruiz del Arbol, M. Masciovecchio, D. Meister, P. Musella, F. Nessi-Tedaldi, F. Pandolfi, J. Pata, F. Pauss, L. Perrozzi, M. Peruzzi, M. Quittnat, M. Rossini, A. Starodumov[43], M. Takahashi, V.R. Tavolaro, K. Theofilatos, R. Wallny, H.A. Weber

Universität Zürich, Zurich, Switzerland
T.K. Aarrestad, C. Amsler[44], L. Caminada, M.F. Canelli, V. Chiochia, A. De Cosa, C. Galloni, A. Hinzmann, T. Hreus, B. Kilminster, C. Lange, J. Ngadiuba, D. Pinna, P. Robmann, F.J. Ronga, D. Salerno, S. Taroni, Y. Yang

National Central University, Chung-Li, Taiwan
M. Cardaci, K.H. Chen, T.H. Doan, C. Ferro, Sh. Jain, M. Konyushikhin, C.M. Kuo, W. Lin, Y.J. Lu, R. Volpe, S.S. Yu

National Taiwan University (NTU), Taipei, Taiwan
R. Bartek, P. Chang, Y.H. Chang, Y.W. Chang, Y. Chao, K.F. Chen, P.H. Chen, C. Dietz, F. Fiori, U. Grundler, W.-S. Hou, Y. Hsiung, Y.F. Liu, R.-S. Lu, M. Miñano Moya, E. Petrakou, J.F. Tsai, Y.M. Tzeng

Chulalongkorn University, Faculty of Science, Department of Physics, Bangkok, Thailand
B. Asavapibhop, K. Kovitanggoon, G. Singh, N. Srimanobhas, N. Suwonjandee

Cukurova University, Adana, Turkey
A. Adiguzel, M.N. Bakirci[45], C. Dozen, I. Dumanoglu, E. Eskut, S. Girgis, G. Gokbulut, Y. Guler, E. Gurpinar, I. Hos, E.E. Kangal[46], A. Kayis Topaksu, G. Onengut[47], K. Ozdemir[48], A. Polatoz, D. Sunar Cerci[49], M. Vergili, C. Zorbilmez

Middle East Technical University, Physics Department, Ankara, Turkey
I.V. Akin, B. Bilin, S. Bilmis, B. Isildak[50], G. Karapinar[51], U.E. Surat, M. Yalvac, M. Zeyrek

Bogazici University, Istanbul, Turkey
E.A. Albayrak[52], E. Gülmez, M. Kaya[53], O. Kaya[54], T. Yetkin[55]

Istanbul Technical University, Istanbul, Turkey
K. Cankocak, S. Sen[56], F.I. Vardarlı

Institute for Scintillation Materials of National Academy of Science of Ukraine, Kharkov, Ukraine
B. Grynyov

National Scientific Center, Kharkov Institute of Physics and Technology, Kharkov, Ukraine
L. Levchuk, P. Sorokin

University of Bristol, Bristol, United Kingdom
R. Aggleton, F. Ball, L. Beck, J.J. Brooke, E. Clement, D. Cussans, H. Flacher, J. Goldstein, M. Grimes, G.P. Heath, H.F. Heath, J. Jacob, L. Kreczko, C. Lucas, Z. Meng, D.M. Newbold[57], S. Paramesvaran, A. Poll, T. Sakuma, S. Seif El Nasr-storey, S. Senkin, D. Smith, V.J. Smith

Rutherford Appleton Laboratory, Didcot, United Kingdom
K.W. Bell, A. Belyaev[58], C. Brew, R.M. Brown, D.J.A. Cockerill, J.A. Coughlan, K. Harder, S. Harper, E. Olaiya, D. Petyt, C.H. Shepherd-Themistocleous, A. Thea, L. Thomas, I.R. Tomalin, T. Williams, W.J. Womersley, S.D. Worm

Imperial College, London, United Kingdom
M. Baber, R. Bainbridge, O. Buchmuller, A. Bundock, D. Burton, S. Casasso, M. Citron, D. Colling, L. Corpe, N. Cripps, P. Dauncey, G. Davies, A. De Wit, M. Della Negra, P. Dunne, A. Elwood, W. Ferguson, J. Fulcher, D. Futyan, G. Hall, G. Iles, G. Karapostoli, M. Kenzie, R. Lane, R. Lucas[57], L. Lyons, A.-M. Magnan, S. Malik, J. Nash, A. Nikitenko[43], J. Pela, M. Pesaresi, K. Petridis, D.M. Raymond, A. Richards, A. Rose, C. Seez, A. Tapper, K. Uchida, M. Vazquez Acosta[59], T. Virdee, S.C. Zenz

Brunel University, Uxbridge, United Kingdom
J.E. Cole, P.R. Hobson, A. Khan, P. Kyberd, D. Leggat, D. Leslie, I.D. Reid, P. Symonds, L. Teodorescu, M. Turner

Baylor University, Waco, USA
A. Borzou, K. Call, J. Dittmann, K. Hatakeyama, A. Kasmi, H. Liu, N. Pastika

The University of Alabama, Tuscaloosa, USA
O. Charaf, S.I. Cooper, C. Henderson, P. Rumerio

Boston University, Boston, USA
A. Avetisyan, T. Bose, C. Fantasia, D. Gastler, P. Lawson, D. Rankin, C. Richardson, J. Rohlf, J. St. John, L. Sulak, D. Zou

Brown University, Providence, USA
J. Alimena, E. Berry, S. Bhattacharya, D. Cutts, N. Dhingra, A. Ferapontov, A. Garabedian, U. Heintz, E. Laird, G. Landsberg, Z. Mao, M. Narain, S. Sagir, T. Sinthuprasith

University of California, Davis, Davis, USA
R. Breedon, G. Breto, M. Calderon De La Barca Sanchez, S. Chauhan, M. Chertok, J. Conway, R. Conway, P.T. Cox, R. Erbacher, M. Gardner, W. Ko, R. Lander, M. Mulhearn, D. Pellett, J. Pilot, F. Ricci-Tam, S. Shalhout, J. Smith, M. Squires, D. Stolp, M. Tripathi, S. Wilbur, R. Yohay

University of California, Los Angeles, USA
R. Cousins, P. Everaerts, C. Farrell, J. Hauser, M. Ignatenko, D. Saltzberg, E. Takasugi, V. Valuev, M. Weber

University of California, Riverside, Riverside, USA
K. Burt, R. Clare, J. Ellison, J.W. Gary, G. Hanson, J. Heilman, M. Ivova PANEVA, P. Jandir, E. Kennedy, F. Lacroix, O.R. Long, A. Luthra, M. Malberti, M. Olmedo Negrete, A. Shrinivas, H. Wei, S. Wimpenny

University of California, San Diego, La Jolla, USA
J.G. Branson, G.B. Cerati, S. Cittolin, R.T. D'Agnolo, A. Holzner, R. Kelley, D. Klein, J. Letts, I. Macneill, D. Olivito, S. Padhi, M. Pieri, M. Sani, V. Sharma, S. Simon, M. Tadel, A. Vartak, S. Wasserbaech[60], C. Welke, F. Würthwein, A. Yagil, G. Zevi Della Porta

University of California, Santa Barbara, Santa Barbara, USA
D. Barge, J. Bradmiller-Feld, C. Campagnari, A. Dishaw, V. Dutta, K. Flowers, M. Franco Sevilla, P. Geffert, C. George, F. Golf, L. Gouskos, J. Gran, J. Incandela, C. Justus, N. Mccoll, S.D. Mullin, J. Richman, D. Stuart, I. Suarez, W. To, C. West, J. Yoo

California Institute of Technology, Pasadena, USA
D. Anderson, A. Apresyan, A. Bornheim, J. Bunn, Y. Chen, J. Duarte, A. Mott, H.B. Newman, C. Pena, M. Pierini, M. Spiropulu, J.R. Vlimant, S. Xie, R.Y. Zhu

Carnegie Mellon University, Pittsburgh, USA
V. Azzolini, A. Calamba, B. Carlson, T. Ferguson, Y. Iiyama, M. Paulini, J. Russ, M. Sun, H. Vogel, I. Vorobiev

University of Colorado Boulder, Boulder, USA
J.P. Cumalat, W.T. Ford, A. Gaz, F. Jensen, A. Johnson, M. Krohn, T. Mulholland, U. Nauenberg, J.G. Smith, K. Stenson, S.R. Wagner

Cornell University, Ithaca, USA
J. Alexander, A. Chatterjee, J. Chaves, J. Chu, S. Dittmer, N. Eggert, N. Mirman, G. Nicolas Kaufman, J.R. Patterson, A. Rinkevicius, A. Ryd, L. Skinnari, L. Soffi, W. Sun, S.M. Tan, W.D. Teo, J. Thom, J. Thompson, J. Tucker, Y. Weng, P. Wittich

Fermi National Accelerator Laboratory, Batavia, USA
S. Abdullin, M. Albrow, J. Anderson, G. Apollinari, L.A.T. Bauerdick, A. Beretvas, J. Berryhill, P.C. Bhat, G. Bolla, K. Burkett, J.N. Butler, H.W.K. Cheung, F. Chlebana, S. Cihangir, V.D. Elvira, I. Fisk, J. Freeman, E. Gottschalk, L. Gray, D. Green, S. Grünendahl, O. Gutsche, J. Hanlon, D. Hare, R.M. Harris, J. Hirschauer, B. Hooberman, Z. Hu, S. Jindariani, M. Johnson, U. Joshi, A.W. Jung, B. Klima, B. Kreis, S. Kwan[†], S. Lammel, J. Linacre, D. Lincoln, R. Lipton,

T. Liu, R. Lopes De Sá, J. Lykken, K. Maeshima, J.M. Marraffino, V.I. Martinez Outschoorn, S. Maruyama, D. Mason, P. McBride, P. Merkel, K. Mishra, S. Mrenna, S. Nahn, C. Newman-Holmes, V. O'Dell, K. Pedro, O. Prokofyev, G. Rakness, E. Sexton-Kennedy, A. Soha, W.J. Spalding, L. Spiegel, L. Taylor, S. Tkaczyk, N.V. Tran, L. Uplegger, E.W. Vaandering, C. Vernieri, M. Verzocchi, R. Vidal, A. Whitbeck, F. Yang, H. Yin

University of Florida, Gainesville, USA
D. Acosta, P. Avery, P. Bortignon, D. Bourilkov, A. Carnes, M. Carver, D. Curry, S. Das, G.P. Di Giovanni, R.D. Field, M. Fisher, I.K. Furic, J. Hugon, J. Konigsberg, A. Korytov, J.F. Low, P. Ma, K. Matchev, H. Mei, P. Milenovic[61], G. Mitselmakher, L. Muniz, D. Rank, R. Rossin, L. Shchutska, M. Snowball, D. Sperka, J. Wang, S. Wang, J. Yelton

Florida International University, Miami, USA
S. Hewamanage, S. Linn, P. Markowitz, G. Martinez, J.L. Rodriguez

Florida State University, Tallahassee, USA
A. Ackert, J.R. Adams, T. Adams, A. Askew, J. Bochenek, B. Diamond, J. Haas, S. Hagopian, V. Hagopian, K.F. Johnson, A. Khatiwada, H. Prosper, V. Veeraraghavan, M. Weinberg

Florida Institute of Technology, Melbourne, USA
V. Bhopatkar, M. Hohlmann, H. Kalakhety, D. Mareskas-palcek, T. Roy, F. Yumiceva

University of Illinois at Chicago (UIC), Chicago, USA
M.R. Adams, L. Apanasevich, D. Berry, R.R. Betts, I. Bucinskaite, R. Cavanaugh, O. Evdokimov, L. Gauthier, C.E. Gerber, D.J. Hofman, P. Kurt, C. O'Brien, I.D. Sandoval Gonzalez, C. Silkworth, P. Turner, N. Varelas, Z. Wu, M. Zakaria

The University of Iowa, Iowa City, USA
B. Bilki[62], W. Clarida, K. Dilsiz, S. Durgut, R.P. Gandrajula, M. Haytmyradov, V. Khristenko, J.-P. Merlo, H. Mermerkaya[63], A. Mestvirishvili, A. Moeller, J. Nachtman, H. Ogul, Y. Onel, F. Ozok[52], A. Penzo, C. Snyder, P. Tan, E. Tiras, J. Wetzel, K. Yi

Johns Hopkins University, Baltimore, USA
I. Anderson, B.A. Barnett, B. Blumenfeld, D. Fehling, L. Feng, A.V. Gritsan, P. Maksimovic, C. Martin, K. Nash, M. Osherson, M. Swartz, M. Xiao, Y. Xin

The University of Kansas, Lawrence, USA
P. Baringer, A. Bean, G. Benelli, C. Bruner, J. Gray, R.P. Kenny III, D. Majumder, M. Malek, M. Murray, D. Noonan, S. Sanders, R. Stringer, Q. Wang, J.S. Wood

Kansas State University, Manhattan, USA
I. Chakaberia, A. Ivanov, K. Kaadze, S. Khalil, M. Makouski, Y. Maravin, A. Mohammadi, L.K. Saini, N. Skhirtladze, I. Svintradze, S. Toda

Lawrence Livermore National Laboratory, Livermore, USA
D. Lange, F. Rebassoo, D. Wright

University of Maryland, College Park, USA
C. Anelli, A. Baden, O. Baron, A. Belloni, B. Calvert, S.C. Eno, C. Ferraioli, J.A. Gomez, N.J. Hadley, S. Jabeen, R.G. Kellogg, T. Kolberg, J. Kunkle, Y. Lu, A.C. Mignerey, Y.H. Shin, A. Skuja, M.B. Tonjes, S.C. Tonwar

Massachusetts Institute of Technology, Cambridge, USA
A. Apyan, R. Barbieri, A. Baty, K. Bierwagen, S. Brandt, W. Busza, I.A. Cali, Z. Demiragli, L. Di Matteo, G. Gomez Ceballos, M. Goncharov, D. Gulhan, G.M. Innocenti, M. Klute, D. Kovalskyi,

Y.S. Lai, Y.-J. Lee, A. Levin, P.D. Luckey, C. Mcginn, C. Mironov, X. Niu, C. Paus, D. Ralph, C. Roland, G. Roland, J. Salfeld-Nebgen, G.S.F. Stephans, K. Sumorok, M. Varma, D. Velicanu, J. Veverka, J. Wang, T.W. Wang, B. Wyslouch, M. Yang, V. Zhukova

University of Minnesota, Minneapolis, USA
B. Dahmes, A. Finkel, A. Gude, P. Hansen, S. Kalafut, S.C. Kao, K. Klapoetke, Y. Kubota, Z. Lesko, J. Mans, S. Nourbakhsh, N. Ruckstuhl, R. Rusack, N. Tambe, J. Turkewitz

University of Mississippi, Oxford, USA
J.G. Acosta, S. Oliveros

University of Nebraska-Lincoln, Lincoln, USA
E. Avdeeva, K. Bloom, S. Bose, D.R. Claes, A. Dominguez, C. Fangmeier, R. Gonzalez Suarez, R. Kamalieddin, J. Keller, D. Knowlton, I. Kravchenko, J. Lazo-Flores, F. Meier, J. Monroy, F. Ratnikov, J.E. Siado, G.R. Snow

State University of New York at Buffalo, Buffalo, USA
M. Alyari, J. Dolen, J. George, A. Godshalk, I. Iashvili, J. Kaisen, A. Kharchilava, A. Kumar, S. Rappoccio

Northeastern University, Boston, USA
G. Alverson, E. Barberis, D. Baumgartel, M. Chasco, A. Hortiangtham, A. Massironi, D.M. Morse, D. Nash, T. Orimoto, R. Teixeira De Lima, D. Trocino, R.-J. Wang, D. Wood, J. Zhang

Northwestern University, Evanston, USA
K.A. Hahn, A. Kubik, N. Mucia, N. Odell, B. Pollack, A. Pozdnyakov, M. Schmitt, S. Stoynev, K. Sung, M. Trovato, M. Velasco, S. Won

University of Notre Dame, Notre Dame, USA
A. Brinkerhoff, N. Dev, M. Hildreth, C. Jessop, D.J. Karmgard, N. Kellams, K. Lannon, S. Lynch, N. Marinelli, F. Meng, C. Mueller, Y. Musienko[33], T. Pearson, M. Planer, A. Reinsvold, R. Ruchti, G. Smith, N. Valls, M. Wayne, M. Wolf, A. Woodard

The Ohio State University, Columbus, USA
L. Antonelli, J. Brinson, B. Bylsma, L.S. Durkin, S. Flowers, A. Hart, C. Hill, R. Hughes, K. Kotov, T.Y. Ling, B. Liu, W. Luo, D. Puigh, M. Rodenburg, B.L. Winer, H.W. Wulsin

Princeton University, Princeton, USA
O. Driga, P. Elmer, J. Hardenbrook, P. Hebda, S.A. Koay, P. Lujan, D. Marlow, T. Medvedeva, M. Mooney, J. Olsen, C. Palmer, P. Piroué, X. Quan, H. Saka, D. Stickland, C. Tully, J.S. Werner, A. Zuranski

University of Puerto Rico, Mayaguez, USA
S. Malik

Purdue University, West Lafayette, USA
V.E. Barnes, D. Benedetti, D. Bortoletto, L. Gutay, M.K. Jha, M. Jones, K. Jung, M. Kress, D.H. Miller, N. Neumeister, F. Primavera, B.C. Radburn-Smith, X. Shi, I. Shipsey, D. Silvers, J. Sun, A. Svyatkovskiy, F. Wang, W. Xie, L. Xu, J. Zablocki

Purdue University Calumet, Hammond, USA
N. Parashar, J. Stupak

Rice University, Houston, USA
A. Adair, B. Akgun, Z. Chen, K.M. Ecklund, F.J.M. Geurts, M. Guilbaud, W. Li, B. Michlin, M. Northup, B.P. Padley, R. Redjimi, J. Roberts, J. Rorie, Z. Tu, J. Zabel

University of Rochester, Rochester, USA
B. Betchart, A. Bodek, P. de Barbaro, R. Demina, Y. Eshaq, T. Ferbel, M. Galanti, A. Garcia-Bellido, P. Goldenzweig, J. Han, A. Harel, O. Hindrichs, A. Khukhunaishvili, G. Petrillo, M. Verzetti

The Rockefeller University, New York, USA
L. Demortier

Rutgers, The State University of New Jersey, Piscataway, USA
S. Arora, A. Barker, J.P. Chou, C. Contreras-Campana, E. Contreras-Campana, D. Duggan, D. Ferencek, Y. Gershtein, R. Gray, E. Halkiadakis, D. Hidas, E. Hughes, S. Kaplan, R. Kunnawalkam Elayavalli, A. Lath, S. Panwalkar, M. Park, S. Salur, S. Schnetzer, D. Sheffield, S. Somalwar, R. Stone, S. Thomas, P. Thomassen, M. Walker

University of Tennessee, Knoxville, USA
M. Foerster, G. Riley, K. Rose, S. Spanier, A. York

Texas A&M University, College Station, USA
O. Bouhali[64], A. Castaneda Hernandez, M. Dalchenko, M. De Mattia, A. Delgado, S. Dildick, R. Eusebi, W. Flanagan, J. Gilmore, T. Kamon[65], V. Krutelyov, R. Montalvo, R. Mueller, I. Osipenkov, Y. Pakhotin, R. Patel, A. Perloff, J. Roe, A. Rose, A. Safonov, A. Tatarinov, K.A. Ulmer[2]

Texas Tech University, Lubbock, USA
N. Akchurin, C. Cowden, J. Damgov, C. Dragoiu, P.R. Dudero, J. Faulkner, S. Kunori, K. Lamichhane, S.W. Lee, T. Libeiro, S. Undleeb, I. Volobouev

Vanderbilt University, Nashville, USA
E. Appelt, A.G. Delannoy, S. Greene, A. Gurrola, R. Janjam, W. Johns, C. Maguire, Y. Mao, A. Melo, P. Sheldon, B. Snook, S. Tuo, J. Velkovska, Q. Xu

University of Virginia, Charlottesville, USA
M.W. Arenton, S. Boutle, B. Cox, B. Francis, J. Goodell, R. Hirosky, A. Ledovskoy, H. Li, C. Lin, C. Neu, E. Wolfe, J. Wood, F. Xia

Wayne State University, Detroit, USA
C. Clarke, R. Harr, P.E. Karchin, C. Kottachchi Kankanamge Don, P. Lamichhane, J. Sturdy

University of Wisconsin, Madison, USA
D.A. Belknap, D. Carlsmith, M. Cepeda, A. Christian, S. Dasu, L. Dodd, S. Duric, E. Friis, B. Gomber, M. Grothe, R. Hall-Wilton, M. Herndon, A. Hervé, P. Klabbers, A. Lanaro, A. Levine, K. Long, R. Loveless, A. Mohapatra, I. Ojalvo, T. Perry, G.A. Pierro, G. Polese, I. Ross, T. Ruggles, T. Sarangi, A. Savin, A. Sharma, N. Smith, W.H. Smith, D. Taylor, N. Woods

†: Deceased
1: Also at Vienna University of Technology, Vienna, Austria
2: Also at CERN, European Organization for Nuclear Research, Geneva, Switzerland
3: Also at State Key Laboratory of Nuclear Physics and Technology, Peking University, Beijing, China
4: Also at Institut Pluridisciplinaire Hubert Curien, Université de Strasbourg, Université de Haute Alsace Mulhouse, CNRS/IN2P3, Strasbourg, France

5: Also at National Institute of Chemical Physics and Biophysics, Tallinn, Estonia
6: Also at Skobeltsyn Institute of Nuclear Physics, Lomonosov Moscow State University, Moscow, Russia
7: Also at Universidade Estadual de Campinas, Campinas, Brazil
8: Also at Centre National de la Recherche Scientifique (CNRS) - IN2P3, Paris, France
9: Also at Laboratoire Leprince-Ringuet, Ecole Polytechnique, IN2P3-CNRS, Palaiseau, France
10: Also at Joint Institute for Nuclear Research, Dubna, Russia
11: Also at Zewail City of Science and Technology, Zewail, Egypt
12: Also at Ain Shams University, Cairo, Egypt
13: Now at British University in Egypt, Cairo, Egypt
14: Also at Helwan University, Cairo, Egypt
15: Also at Université de Haute Alsace, Mulhouse, France
16: Also at Tbilisi State University, Tbilisi, Georgia
17: Also at Brandenburg University of Technology, Cottbus, Germany
18: Also at Institute of Nuclear Research ATOMKI, Debrecen, Hungary
19: Also at Eötvös Loránd University, Budapest, Hungary
20: Also at University of Debrecen, Debrecen, Hungary
21: Also at Wigner Research Centre for Physics, Budapest, Hungary
22: Also at University of Visva-Bharati, Santiniketan, India
23: Now at King Abdulaziz University, Jeddah, Saudi Arabia
24: Also at University of Ruhuna, Matara, Sri Lanka
25: Also at Isfahan University of Technology, Isfahan, Iran
26: Also at University of Tehran, Department of Engineering Science, Tehran, Iran
27: Also at Plasma Physics Research Center, Science and Research Branch, Islamic Azad University, Tehran, Iran
28: Also at Università degli Studi di Siena, Siena, Italy
29: Also at Purdue University, West Lafayette, USA
30: Also at International Islamic University of Malaysia, Kuala Lumpur, Malaysia
31: Also at Malaysian Nuclear Agency, MOSTI, Kajang, Malaysia
32: Also at Consejo Nacional de Ciencia y Tecnología, Mexico city, Mexico
33: Also at Institute for Nuclear Research, Moscow, Russia
34: Also at St. Petersburg State Polytechnical University, St. Petersburg, Russia
35: Also at National Research Nuclear University 'Moscow Engineering Physics Institute' (MEPhI), Moscow, Russia
36: Also at California Institute of Technology, Pasadena, USA
37: Also at Faculty of Physics, University of Belgrade, Belgrade, Serbia
38: Also at Facoltà Ingegneria, Università di Roma, Roma, Italy
39: Also at National Technical University of Athens, Athens, Greece
40: Also at Scuola Normale e Sezione dell'INFN, Pisa, Italy
41: Also at University of Athens, Athens, Greece
42: Also at Warsaw University of Technology, Institute of Electronic Systems, Warsaw, Poland
43: Also at Institute for Theoretical and Experimental Physics, Moscow, Russia
44: Also at Albert Einstein Center for Fundamental Physics, Bern, Switzerland
45: Also at Gaziosmanpasa University, Tokat, Turkey
46: Also at Mersin University, Mersin, Turkey
47: Also at Cag University, Mersin, Turkey
48: Also at Piri Reis University, Istanbul, Turkey
49: Also at Adiyaman University, Adiyaman, Turkey
50: Also at Ozyegin University, Istanbul, Turkey

51: Also at Izmir Institute of Technology, Izmir, Turkey
52: Also at Mimar Sinan University, Istanbul, Istanbul, Turkey
53: Also at Marmara University, Istanbul, Turkey
54: Also at Kafkas University, Kars, Turkey
55: Also at Yildiz Technical University, Istanbul, Turkey
56: Also at Hacettepe University, Ankara, Turkey
57: Also at Rutherford Appleton Laboratory, Didcot, United Kingdom
58: Also at School of Physics and Astronomy, University of Southampton, Southampton, United Kingdom
59: Also at Instituto de Astrofísica de Canarias, La Laguna, Spain
60: Also at Utah Valley University, Orem, USA
61: Also at University of Belgrade, Faculty of Physics and Vinca Institute of Nuclear Sciences, Belgrade, Serbia
62: Also at Argonne National Laboratory, Argonne, USA
63: Also at Erzincan University, Erzincan, Turkey
64: Also at Texas A&M University at Qatar, Doha, Qatar
65: Also at Kyungpook National University, Daegu, Korea